UCL Université catholique de Louvain

École polytechnique de Louvain (EPL)

epl

Numerical study of powder electrification during pneumatic transport

Dissertation presented by
Lise CERESIAT

for obtaining the Master's degree in
Chemical and Materials Engineering

Supervisor
Miltiadis PAPALEXANDRIS

Readers
Juray DE WILDE, Sandra SOARES FRAZAO , Holger GROSSHANS

Academic year 2017-2018

Contents

Introduction and objectives

During pneumatic transports, powders often face to buildup of electrostatic charge on their surface due to the wall-collisions of the particles against the pipe. This phenomenon can lead to hazardous spark discharges and dust explosions that are unwanted implications. A strong interest on the subject exists to understand the way the powders charging occurs and to determine the parameters affecting it.

In the literature, many experimental studies and numerical investigations have been made. They concluded that the contact electrification depends on several parameters, as for example the transport regime, the materials of the pipe and the powder, the temperature, etc. Because of that, the ability of experiment to be reproducible is weak. Another conclusion is the strong link between the conveying conditions and the electrification of the powder. The development of the field of Computational Fluid Dynamics made the numerical simulations a helpful tool to model the flow and also the interaction with the powder.

The purpose of this master thesis is to understand how the electrification of the powder is affected by the following parameters : the particles diameter, the particles mass flow rate inside the pipe, the particles material and finally the fluid velocity. The results of these simulations were analyzed to understand the role of the powder size, the physical properties and the converging air velocity on the triboelectric-charging. These results were compared with experiments found in the literature to verify the good prediction of the numerical model.

The first chapter of this work presents the mathematical model to explain the powders electrification. During impact with the wall, the system can be modeled as a charging-discharging capacitor and, during the contact, an electron(s) transfer can be supposed for explaining the charge exchange. The second chapter presents the results of the different simulations. First, the nominal powder results are explained. After that, the results about the diameter variations, the mass flow rate variations, the different type of materials powder and the fluid velocity variations are explained. Each of them is compared to the nominal case to understand the way the electrification is affected by the parameter of the simulation. The third chapter compares the simulations results with some experiments measures found in the literature. At the end, a conclusion is presented based on the obtained results described in this work.

Chapter 1

Mathematical model

In this section[1], the mathematical model of the electrification of a powder during pneumatic transport will be given. Initially, the particles are injected in the pipe without electrical pre-charge on their surface and travel through it with the help of a fluid at high velocity. Due to this velocity and the small diameter of the pipe, the transport regime is turbulent and the particles collide either with the wall or between themselves. Since the powder and the wall are made of different materials, they have different work functions and when a contact occurs, a transfer of charge happens to equalize the level of energy of both material [5]. This is by definition the triboelectric effect.

In this work, the system is composed of a circular steel pipe and of a powder made of polymer materials. The transport fluid is air and it is considered incompressible with constant physical properties. The description of the flow is based on Navier-Stokes equations. These ones are solved in Eulerian framework for the fluid phase and in Lagrangien framework for the solid phase so as to explain the motion of each particle. The flow through the pipe is considered to be diluted, meaning the volume fraction of particles is low compared to the volume fraction of the fluid.

At first, the description of the fluid phase acceleration is given, followed by the description of the solid phase acceleration with the description of the forces acting on it. Finally, the different mechanisms of charge transfer are developed in more details to understand the way the particles become electrically charged during transport and which parameters could affect this charge.

1.1 Governing equations of the fluid phase

With the previous assumptions, the mass and the momentum balances can be calculated. This gives the Navier-Stokes equations with a source term for the interphasial drag :

[1]This section is based on [1], [2], [3] and [4]

$$\nabla \cdot \mathbf{u} = 0, \tag{1.1}$$

$$\frac{\partial \mathbf{u}}{\partial t} + (\mathbf{u} \cdot \nabla)\mathbf{u} = -\frac{1}{\rho}\nabla p + \nu \nabla^2 \mathbf{u} + F_s, \tag{1.2}$$

where $\mathbf{u}$ = (u, v, w) is the fluid velocity vector. The parameters p, ρ and ν represent respectively the pressure, the density and the kinematic viscosity of to the fluid. The last term, F_s, is the source term that takes into account the momentum transfer between the two phases. These equations are valid for all domains.

1.2 Balance of force on the particles

The flow of the particles is based on several assumptions: the particle are considered to be isolated from each other, rigid and have a spherical shape. All the particles are supposed to be made of the same material, and to have the same physical properties including their diameter. With these hypotheses, the acceleration of one particle can be described based on its velocity $\mathbf{u}_p$ as follow:

$$\frac{d\mathbf{u}_p}{dt} = \mathbf{f}_{aero} + \mathbf{f}_g + \mathbf{f}_{coll} + \mathbf{f}_{el}. \tag{1.3}$$

In this expression, each term $\mathbf{f}_{aero}$, $\mathbf{f}_g$, $\mathbf{f}_{coll}$ and $\mathbf{f}_{el}$ represents the acceleration due respectively to the aerodynamic drag force, the gravitational force, the collisional force and the electric field force acting on the particle. The collisional force takes into account two phenomena: collisions between particles and collisions with the inner wall of the pipe. Each term of 1.3 is detailed below.

(i) The acceleration due to gravity is given by

$$\mathbf{f}_g = \left(1 - \frac{\rho}{\rho_p}\right)\mathbf{g}, \tag{1.4}$$

where $\mathbf{g}$ is the gravitational acceleration, and ρ and ρ_p are the densities of the fluid and of the particle respectively.

(ii) The aerodynamic drag forces are given by:

$$\mathbf{f}_{aero} = -\frac{3\rho}{8\rho_p r_p} C_d |\mathbf{u}_{rel}| \mathbf{u}_{rel}, \tag{1.5}$$

where $\mathbf{u}_{rel}$ is the particle velocity relative to the fluid, $\mathbf{u}_{rel} = \mathbf{u}_p$ - $\mathbf{u}$. C_d is the drag coefficient of the particles and is a function of the particle Reynolds number $Re_p = 2|\mathbf{u}_{rel}|r_p/\nu$. C_d is calculated with the correlation proposed by Schiller & Naumann [6] :

$$\begin{cases} C_d = \frac{4}{Re_p}(6 + Re_p^{2/3}) & \text{for } \mathrm{Re}_p \leq 1000, \quad (1.6) \\ \mathrm{C}_d = 0.424 & \text{for } \mathrm{Re}_p > 1000. \quad (1.7) \end{cases}$$

(iii) The collisional forces depend of two types of collisions: between the particles and with the wall. The first type is considered to be fully elastic. This assumption means that the momentum and the kinetic energy are conserved. Looking at one collision between two particles with respectively index 1 and 2, these relations can be written as

$$\begin{cases} \rho_p V_{p,1} \mathbf{u'}_{p,1} + \rho_p V_{p,2} \mathbf{u'}_{p,2} = \rho_p V_{p,1} \mathbf{u''}_{p,1} + \rho_p V_{p,2} \mathbf{u''}_{p,2}, & (1.8) \\ \frac{\rho_p V_{p,1} \mathbf{u'}_{p,1}^2}{2} + \frac{\rho_p V_{p,2} \mathbf{u'}_{p,2}^2}{2} = \frac{\rho_p V_{p,1} \mathbf{u''}_{p,1}^2}{2} + \frac{\rho_p V_{p,2} \mathbf{u''}_{p,2}^2}{2}. & (1.9) \end{cases}$$

With the previous assumptions of particles made of the same material and with the same dimension, the density ,ρ_p, and the particles volume, $V_{p,i} = 4\pi r_{p,i}^3/3$, can be simplified from these equations. It gives the velocity before and after collision, $\mathbf{u'}_{p,i}$ and $\mathbf{u''}_{p,i}$ respectively. With recombination and simplifications of these two equations, the final velocities of both particles are:

$$\begin{cases} \mathbf{u''}_{p,1} = \frac{(r_{p,1}^3 - r_{p,2}^3)\mathbf{u'}_{p,1} + 2r_{p,2}^3 \mathbf{u'}_{p,2}}{r_{p,1}^3 + r_{p,2}^3}, & (1.10) \\ \mathbf{u''}_{p,2} = \frac{(r_{p,2}^3 - r_{p,1}^3)\mathbf{u'}_{p,2} + 2r_{p,1}^3 \mathbf{u'}_{p,1}}{r_{p,1}^3 + r_{p,2}^3}. & (1.11) \end{cases}$$

These equations are valid for the general case of a powder having a size distribution. Since one assumption made for this work is the equal size and shape of particles, then the radius will be the same between both of them, $r_{p,1} = r_{p,2}$. Particle will then moves faster or slower by being hit by a particles travelling faster or slower respectively.

The second type of collision appears when a particle hits the wall. As said before, both are made of different materials and the particle will undergo a deformation during impact. Due to that, the assumption of elastic collision is no longer valid. Before and after the impact, the velocity of the particle $\mathbf{u}_p$ can be split into two components: normal and tangential with respect to the wall. After collision, the new velocity $\mathbf{u}_p''$ will keep the same tangential component but the normal velocity component changes of sign and amplitude:

$$\begin{cases} \mathbf{u}_p'' \cdot \mathbf{n}_t = \mathbf{u}_p \cdot \mathbf{n}_t, & (1.12) \\ \mathbf{u}_p'' \cdot \mathbf{n}_n = -k_e \mathbf{u}_p \cdot \mathbf{n}_n. & (1.13) \end{cases}$$

The restitution ratio k_e is considered to be a material property of the particles and has been fixed to 0.95 [7].

(iv) The last term of the acceleration in equation 1.3 comes from the charge appearing on a

particle that will produce a local electrical field. This can be expressed as follow :

$$\mathbf{f}_{el} = \frac{Q\mathbf{E}}{m_p}, \tag{1.14}$$

where Q is the electrical charge of the particle and m_p its mass. The electric field $\mathbf{E}$ is given by definition as the gradient of the electric potential :

$$\mathbf{E} = -\nabla V. \tag{1.15}$$

The divergence of the electrical field is equal to the charge density of the particles ρ_{el} divided by the permittivity vacuum, ϵ_0. We suppose that the fluid has the same permittivity as the permittivity vacuum and at the end, this gives the Poisson equation for the electrical potential :

$$\nabla \cdot E = \nabla^2 V = -\frac{\rho_{el}}{\epsilon_0}. \tag{1.16}$$

Gauss's law says that the flux of electric field through a closed surface is equal to the sum of all charges present in the volume contained by this surface. Thus, the charge density can be found by integration over a volume of control V_c containing n particles :

$$\int_{V_c} \rho_{el}\, dV_c = \sum_{i=1}^{n} Q_i. \tag{1.17}$$

1.3 Transfer of charge

As said before, during the powder transport, two types of contacts may occur : a collision between two particles or an impact with the wall [3]. In the case of polymeric powder, the first type of contact can be seen as an insulator-insulator contact while the second one is more related to a metal-insulator contact. Both will undergo a charge transfer via electron(s) transfer at the surface of the materials. The calculation of these transfers is based on the analogy with a capacitor discharge and have been proposed by Soo [8].

1.3.1 Inter-particle collisions

At first, the calculation of the exchange during collisions between the particles is given. The powder is supposed to be made of a homogeneous material and the exchange can only happen when the particles carry different charges on their surface. This means that the net charge of the powder comes only from the impacts with the wall. The collisions between particles will just distribute the charges among the whole powder but will not increase the net charge. For the calculation, we consider a collision between two particles, with index 1 and 2 respectively. The charge exchange during a contact time Δt_p is given by the following equation:

$$\Delta Q_1 = -\Delta Q_2 = \frac{C_1 C_2}{C_1 + C_2}(\frac{Q_2}{C_2} - \frac{Q_1}{C_1})(1 - e^{-\Delta t_p/\tau_p}). \tag{1.18}$$

In this expression, τ_p represents the charge relaxation time, and C_n the electric capacities of the particles 1 and 2, given by the definition :

$$C_n = 4\pi\epsilon_0 r_{p,n}, \tag{1.19}$$

with $r_{p,n}$ the radius of the particle and ϵ_0 the vacuum permittivity. The expression of the charge relaxation time is given by

$$\tau_p = \frac{C_1 C_2}{C_1 + C_2}\frac{r_{p,1} + r_{p,2}}{A_{12}}\phi_p, \tag{1.20}$$

where ϕ_p is the material resistivity and A_{12} the contact area. This surface is calculated with the elastic theory of Hertz to be :

$$A_{12} = \frac{\pi r_{p,1} r_{p,2}}{r_{p,1} + r_{p,2}}\alpha_1. \tag{1.21}$$

The parameter α_1 is the distance between the two spheres at the instant of maximum compression:

$$\alpha_1 = r_{p,1} r_{p,2}\left(\frac{5}{8}\pi\rho_p(1 + k_e)|\mathbf{u}_{p,12}|^2\frac{\sqrt{r_{p,1} + r_{p,2}}}{r_{p,1}^3 + r_{p,2}^3}\frac{1 - \nu_p^2}{E_p}\right)^{2/5}. \tag{1.22}$$

In this expression, $\mathbf{u}_{p,12}$ represents the relative velocity of the two particles: $\mathbf{u}_{p,12}$ = $|\mathbf{u}_{p,2}$ - $\mathbf{u}_{p,1}|$. k_e, ν_p and E_p are particle parameters, respectively the restitution ratio, the Poisson ratio and the Young modulus. It can already be noticed that the exchange will strongly depend on the powder material and on the relative velocity of the particles.

Finally, also given by the theory of Hertz and proposed by Soo [8], the contact time is calculated as follows

$$\Delta t_p = \frac{2.94}{|\mathbf{u}_{p,12}|}\alpha_1. \tag{1.23}$$

The charge exchange of Eq.1.18 can thus be calculated from the above equations.

1.3.2 Wall-particles collisions

The second type of collision is a metal-insulator contact. Because of the difference of the materials, the work functions will also be different, and, during an impact, a potential difference will appear. The work function represents the amount of energy needed to remove one electron from the surface of the material under vacuum [9]. Polymer materials have a higher work function and can be seen like electrons-acceptor in comparison to metals which will more easily give electron(s) during contact. For this reason, the powder will leave the pipe negatively charged. During a collision, the particles will be deformed but since they are supposed to be rigid, the area of contact can be assumed to be smaller than the the main cross section of a particle. With this, the gap between both materials can be represented like a parallel-plate capacitor, illustrated in Figure 1.1.

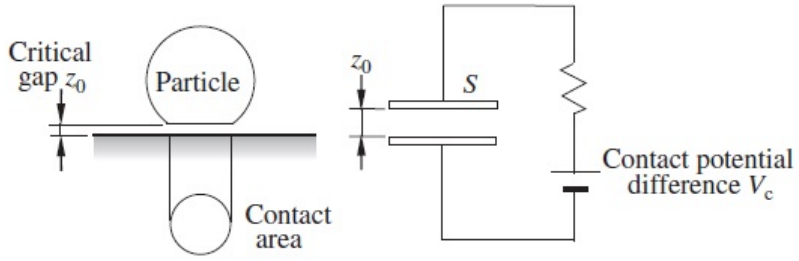

Figure 1.1: Representation of the exchange during collision between a particle and the wall like a parallel-plate capacitor [5].

In this case, the charge exchange has two contributions: the transfer due to the contact potential difference and the transfer due to the initial particle charge :

$$\Delta Q = \Delta Q_c + \Delta Q_t. \tag{1.24}$$

For the contact electrification, the previous model of the charge-discharge of a capacitor can be reused with a correction : the radius of one particle is supposed to be infinite. Then, the exchange of charge during contact is given by

$$\Delta Q_c = C V_c \left(1 - e^{-\Delta t_{pw}/\tau_w}\right). \tag{1.25}$$

In this equation, C, Δt_{pw} and τ_w represent respectively the electrical capacity, the contact time and the charge relaxation time. V_c is the contact potential between the particle and the wall and has been set to 1 V [2]. It is important to note that the value of this potential can be affected by a lot of parameters like the surface roughness, chemical composition of the surface, etc. The electrical capacity for this model is given by :

$$C = \frac{\epsilon_0 A_{pw}}{z_0}, \tag{1.26}$$

where z_0 is the distance between the two capacitor plates (see Fig. 1.1). It represents the effective separation during the collision. Since the surface of the wall is not perfect, z_0 will be in the range of the repulsive molecular force and has been fixed to 10^{-9} m. A_{pw} is the surface of the plate or the contact area and is calculated by the Hertz theory proposed by Soo [8] :

$$A_{pw} = \pi r_p \alpha_2, \tag{1.27}$$

with

$$\alpha_2 = r_p \left(\frac{5}{8}\pi\rho_p(1+k_e)|\mathbf{u}_p|^2 \left(\frac{1-\nu_p^2}{E_p} + \frac{1-\nu_w^2}{E_w}\right)\right)^{2/5}. \tag{1.28}$$

In this equation, index p and w refer to the particles and the wall respectively. The contact time is given by

$$\Delta t_{pw} = \frac{2.94}{|\mathbf{u}_p|}\alpha_2 \tag{1.29}$$

and the charge relaxation time by

$$\tau_w = \epsilon\epsilon_0\phi_p, \tag{1.30}$$

where ϵ is the relative permittivity of the system and is equal to 5.

Finally, the transfer due to the initial particle charge is based on the assumption that the charge is uniformly distributed on its surface. The expression of this transfer as a function of the initial charge of the particle, Q, and the parameter α_2 is :

$$\Delta Q_t = \frac{\alpha_2 Q}{4\ r_p}. \tag{1.31}$$

This second contribution will lower the charge exchange with the wall but since the transported charge is small, this second term is small compared to the term of contact.

To summarise this section, the particles enter the pipe with zero charge on their surface. Some of the particles become electrically charged because of the impacts with the wall and a redistribution of the charges can occur via inter-particles collisions.

1.4 Numerical modelling

The numerical studies of triboelectric charging can be computationally very expensive for a direct numerical simulation, which amounts to resolving all turbulent scales [10]. The dynamics of the flow can be represented in a rather simplified manner. For example, Watano et al.[11] made numerical simulations assuming a pre-defined velocity profile for the fluid. A more realistic approach to performed simulations of triboelectric charging is the Reynolds-average Navier-Stokes (RANS) approach [3]. However, the RANS simulations can only predict the time average velocities and cannot resolve the turbulent structures that are developed in the flow [2]. In Large Eddy Simulations (LES), the large turbulent scales are resolved while the small scales are modeled. LES provided more accurate estimations of the powder electrification. Nevertheless, LES have also uncertainties, especially in the prediction of charge exchange in the near wall regions.

In our work, we performed Large Eddy Simulations by spatially filtering Eqs.1.1 and 1.2 and we obtained the governing equations. They are discretized by the Finite Difference Method. In our model, the small scales unresolved are modeled based on the dynamic Smagorinsky model [12] combined with the least-square technique and averaging of Lilly [13]. The motion of each particles is tracked by the Discrete Element Method. A four-way coupling is assuming to take account the particle-fluid interactions (Eq.1.2) and also the particle-particle interactions via momentum exchange (Eq.1.3). The near-wall flow structures are modelled instead of resolved. The near-wall model is applied assuming that the mean velocity profile follows the logarithmic law.

At the inlet, a velocity profile is chosen which reflects the average profile of a turbulent flow [1].

We used the empirical power-law profile,

$$\frac{u(r)}{u_c} = \left(1 - \frac{2r}{D}\right)^{1/6}, \tag{1.32}$$

for the streamwise velocity component u(r). In this expression, u_c is the centerline velocity and the exponent 1/6 corresponds to a turbulent flow of a moderate intensity. The particles are randomly distributed at the inlet and their velocities are equal to the fluid velocity at the particle locations [3].

The Navier-Stokes equations are not-linear and the three momentum equations (Eq.1.2) are composed of four variables : the pressure and the components of the velocity. These equations are solved with a Pressure-Implicit with Splitting of Operators (PISO) algorithm. First, the pressure is guessed from the previous timestep. Equations 1.2 are solved to find the components of the velocity and, with the solution, the pressure can be calculated. After that a correction is imposed to the flux to respect the continuity. If needed, the schema is iterated [14].

Chapter 2

Simulation results

In this chapter, the results of the different simulations are presented. The powder is continuously injected in a cylinder pipe 4 cm in diameter and 1 m in length. The grid consists of approximately 20 000 points. We have used Cartesian grid and the cylinder is truncate. Its shape is in stair shape instead of perfect circular geometry.

The time scale is 1 second and each simulation gives, at the end, three types of data files. The first one is about the particles at the inlet: the total number of particles and the components of their velocities are given. The second one gives information at the outlet with the total number of particles that have left, their carried charges and the number of collisions with the wall each of them incurred. Finally, the last data file contains information of all the impacts with the wall and shows the values of charge exchanges, contact times and contact areas. The powder is continuously injected and the simulation is stopped when the time scale reaches 1 second. This means that some particles are still inside the pipe and the number of particles at the outlet is different from the number at the inlet.

The electrification of the powder has been studied based on the variations of the following parameters: the particle diameter, the material of the powder, the particle concentration and the fluid velocity. Each case has been compared to the nominal case taken as a powder made of Poly(methyl methacrylate) (PMMA) with a diameter of 300 μm. The injected powder mass flow rate had been set at 10 g/s and the fluid velocity at 30 m/s. First, the results for this sample will be explained.

In a second time, the results coming from the diameter variations will be presented. Three cases were selected for a PMMA powder : 150, 600 and 1200 μm. The electrical charge transport by the powder, the number of collisions with the wall and the exchanges of charges with the pipe will be analyzed for each case. This second part will then conclude by comparing the results for the different simulations.

After that, the effect of the powder concentration will be analyzed via mass flow rate variations.

Two cases were selected: 5 g/s and 50 g/s. It will be followed by the comparison of the electrification of powder made of different materials. For these simulations, the particle size and the mass flow rate were set with the same values as the nominal case. The variations appear via the physical properties of the powder as the Young modulus, the Poisson ratio and the density. Two types of polymer have been chosen: polypropylene (PP) and polycarbonate (PC).

Finally, simulations have been performed at different Reynolds number to look how electrification is affected by the turbulent regime. For this purpose, three fluid velocities were selected: 10, 20 and 40 m/s.

2.1 The nominal case

In this section, the results for the nominal case are presented. The sample taken as reference is made of PMMA with a diameter of 300 μm. The mass flow rate has been set at 10 g/s and the bulk velocity at 30 m/s. In this case, **684 168 particles** are injected continuously in the pipe without any initial charge on their surface. The time scale of the simulation is 1 s. At this time, the simulation is stopped and some particles are still inside the pipe. For this reason, the number of particles at the outlet is different.

2.1.1 Electrical charges on the powder at the outlet

The results of charges carried by the particles found at the outlet of the pipe are summarised in Table 2.1. This table is divided into three sections. The first one gives the fractions of particles that gained electrical charges during the pneumatic transport. More than 80% of them carry charges in the range -5 pC to small values close to 0. The second section gives the distribution on the full range. It was subdivided into charge intervals to show the percentages of particles found in each of them. The average and maximum values of electrical charge can be found in the third section.

Figure 2.1 illustrates these results. The y-axis shows the percentages of particles transporting charges values of the x-axis. Because of the width of the distribution, the graph shows only part of it where nearly 90% of the powder is present. The mean value of charges carried is around -0.02 pC. It can be seen that a majority of the particles transport smaller charges on their surfaces than the average charge. As said in the previous section, two types of collisions can occur : impacts with the wall and inter-particles impacts. The powder becomes electrically charged because of contact with the wall due to the Fermi levels difference and the difference of properties between materials [9]. These exchanges will charge negatively the powder while inter-particle collisions do not change the overall powder charges but redistribute the charges between the particles. Because of that, more particles will transport charges than the number of particles impacting the wall where they receive the charges. In the figure, we can see two parts. The peak on the left represents the carried charges due to the wall impacts. The part close to

zero is the percentage of particles charged due to inter-particle collisions.

	Number of particles	Percentage
Total number of particles found at the outlet	508 450	100 %
Particles carrying charges	414 025	81.43 %
Particles carrying no-charge	94 425	18.57 %
Charge range		
between -5 and -0.05 [pC]	49 964	9.83 %
between -0.05 and -0.025 [pC]	97 684	19.21 %
between -0.025 and -0.005 [pC]	189 007	37.17%
between -0.005 and 0 [pC] (value of 0 exclude)	77 369	15.22 %
	Value	Units
Average value of the charges carried by the particles	-0.0204	pC
Absolute value of the maximum charge carried	3.56	pC

Table 2.1: Collected data about carried charges at the pipe outlet for PMMA powder of 300 μm diameter.

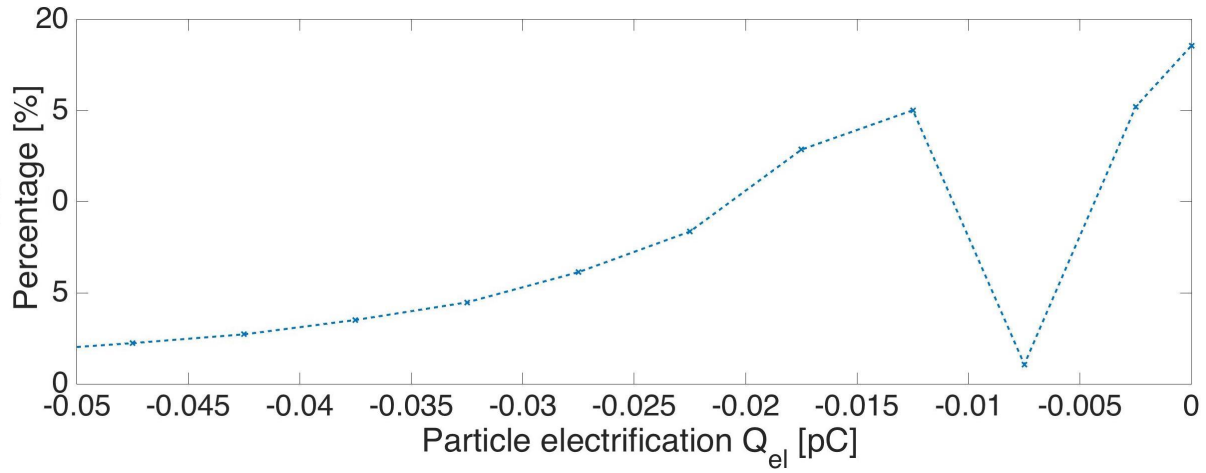

Figure 2.1: Distribution of particle electrification for PMMA powder of 300 μm. The x-axis corresponds to the electric charge. The y-axis corresponds to the percentage of particles carrying a given charge.

2.1.2 Number of collisions with the wall

To have a better distinction between the two types of impact, Table 2.2 shows the number and percentages of particles experiencing a different number of collisions. These numbers are taken at the pipe's outlet. The second part of the table shows the charges gained because of the inter-particle collisions for the particles experiencing no collision with the wall.

In relation with Table 2.1, it can be observed that the interval containing electric charge smaller than -0.005 pC corresponds exactly to the percentage of the powder charged due to inter-particle collisions : 15.22 %. This means that this population comes only from the inter-particles collisions and confirms that this type of interaction gives smaller charge exchange values : the average value of carried charge is smaller by five orders of magnitudes compared to average charge of the

powder.

Number of wall collisions	Number of particles	Percentage
0 collision	171 795	33.79 %
1 collision	279 539	54.98 %
2 collisions	49 289	9.69 %
3 collisions	6 405	1.26 %
more than 4 collisions	1 422	0.28 %
Maximum number of collisions	23	-
Particles undergoing no collision	**Value**	**Units**
Percentage of particles carrying charges	15.22 %	-
Average value of the charges carried	-1.0457e-7	pC
Absolute value of the maximum charge carried	4.48e-4	pC

Table 2.2: Collected data for the number of wall-collisions at the pipe outlet for PMMA powder of 300 μm diameter.

These results are illustrated in Figure 2.2. The graphs show absolute values of the electrical charge. The top graph shows the sum of charges for all particles experiencing a given number of collisions. It represents the charge exchange increase during wall-collisions. In the bottom graph, we have plotted the accumulated wall-particle charge exchange for the powder depending on the number of collisions. This means, for example, that the value at $n_{wc} = 3$ is the accumulated charge value at $n_{wc} = 2$ plus the charge increase at $n_{wc} = 3$.

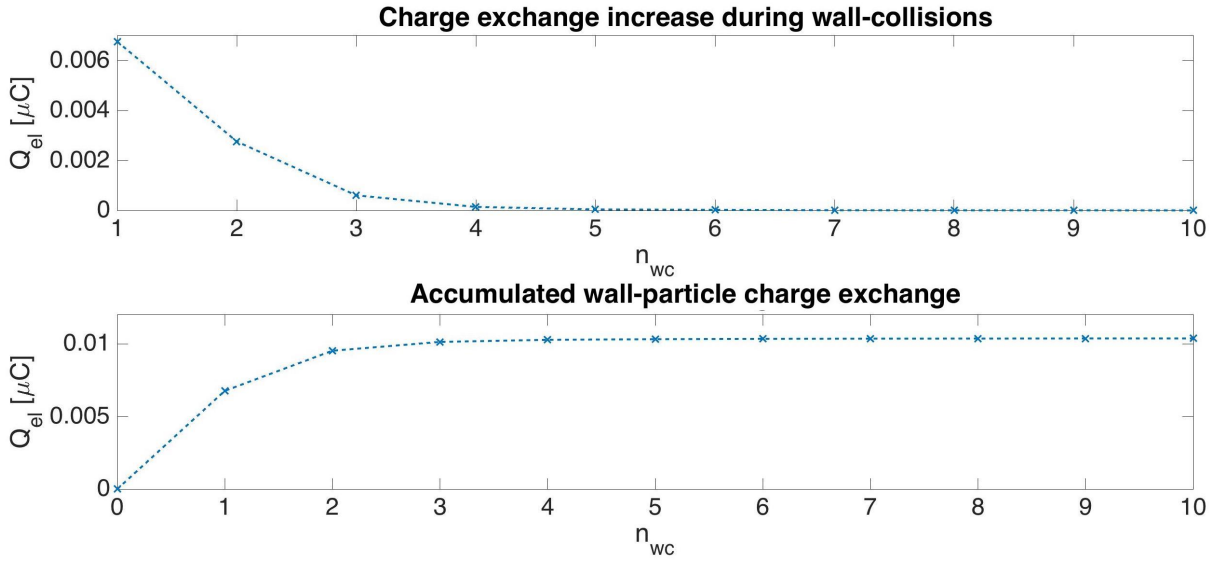

Figure 2.2: Charge exchange increase and accumulated charge exchange during wall-collisions : the accumulated charge at n_{wc} = i is the addition of the accumulated charge at n_{wc} = i-1 and the exchange charge increase at n_{wc} = i.

One must be careful in the interpretation of these graphs since the percentage of particles for each number of collisions is different. Also it is important to remember that these results come from the particles leaving the pipe. Between an impact with the wall and the outlet or between two impacts with the wall, the particles can exchange charges. Nevertheless, we can see that the major contribution to the accumulated charge comes from the particles undergoing one collision.

Even if some particles collide more than three times with the wall, the accumulated charge tends to reach an equilibrium meaning that these impacts do not give important addition of charges to the powder. In this case, the plateau value is **0.0104** μC and the accumulated value for $n_{wc} = 1$ is **0.0068** μC. This represents around 65 % of the final charge of the powder.

2.1.3 Magnitude of the charge exchange during wall-collisions

The results about the charge exchange during the impacts with the wall can be found in Table 2.3. As previously, the range of charge exchange has been divided into different intervals and the percentages of impacts for each range are given in the second section of the table. Figure 2.3 illustrates the distribution density for these exchanges and shows only part of the graph where more than 95% of impacts are included.

	Number of collisions	Percentage
Total number of collisions with the wall	744 578	100 %
Charge range		
between 0 and 0.01 [pC]	20 264	2.72 %
between 0.01 and 0.02 [pC]	361 423	48.54 %
between 0.02 and 0.03 [pC]	183 245	24.61 %
between 0.03 and 0.04 [pC]	91 529	12.3 %
between 0.04 and 0.05 [pC]	44 528	5.98 %
between 0.05 and 5 [pC]	43 589	5.85 %
	Value	Units
Average value of the charge exchange	0.0243	pC
Average area of contact	3.617	nm^2
Average time of contact	30.821	μs
Minimum value of the charge exchange	0.0079	pC
Minimum area of contact	0.864	nm^2
Minimum time of contact	6.87	μs
Maximum value of the charge exchange	3.02	pC
Maximum area of contact	4.66	nm^2
Maximum time of contact	9.6	ms

Table 2.3: Collected data for the charge exchanges during wall collisions for PMMA powder of 300 μm diameter.

This distribution is as broad as the distribution of the charges carried by the particles, the major difference being the disappearance of the region with small values. This correlates well with the observation that smaller values result from the inter-particles collisions.

Because of this, the average value of charge exchange is slightly higher than the average charge carried by the particles, in absolute value. The maximum exchange leads to a high value, a few pC, against the minimum one that is three order of magnitude smaller. The contact time varies also a lot when the contact area stay in the same order of magnitude. Back in Equation1.29 of the previous section, we can see that this difference comes from the norm of the velocity. The contact time will be more sensitive to the difference of velocity and to the speed of the particle

impacting the wall.

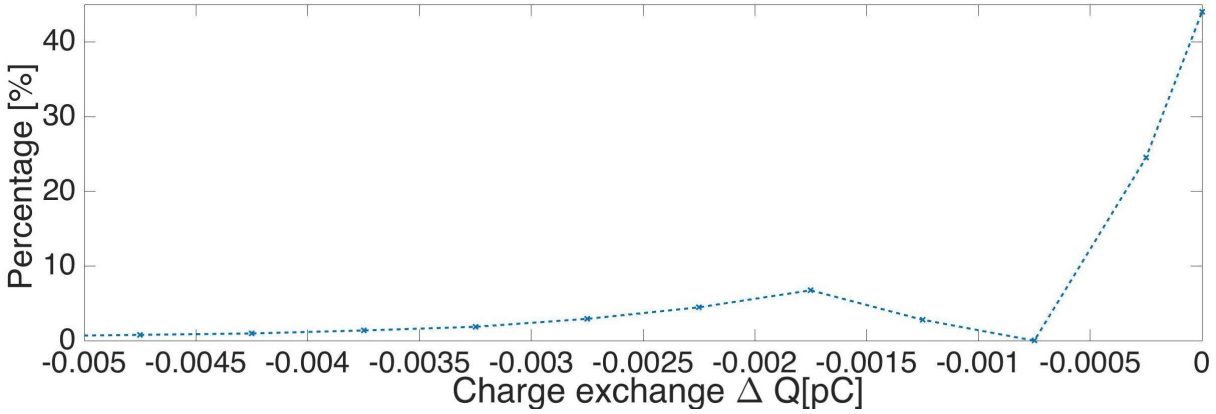

Figure 2.3: Distribution of charge exchange during wall-collisions for PMMA powder of 150 μm. The x-axis corresponds to the charge exchange. The y-axis corresponds to the percentage of exchange resulting a given charge.

2.1.4 3D Visualisation

Finally, the results of the simulation can be visualised in 3D images with the help of the visualisation tool Paraview. This application allows to look at several parameters and how they vary with the time. In our case, we are interested to look at the components of particle velocities and at the electrical charges they transport.

Figures 2.4 and 2.5 show respectively the charges carried by the particles in the axial direction at two different times, respectively 0.03 s and 1 s. The figures are snapshot and show the particles present at this time inside the entire tube of 1 m length and 4 cm diameter. As mentioned before, the range of charge values extends over several order of magnitude. For visualisation purpose, this range was split in two parts and each plot depicts the particles in the corresponding part. The dividing value is -0.025 pC and is close to the average value of the charge. It can be easily seen that a larger number of particles transport smaller magnitudes of charge.

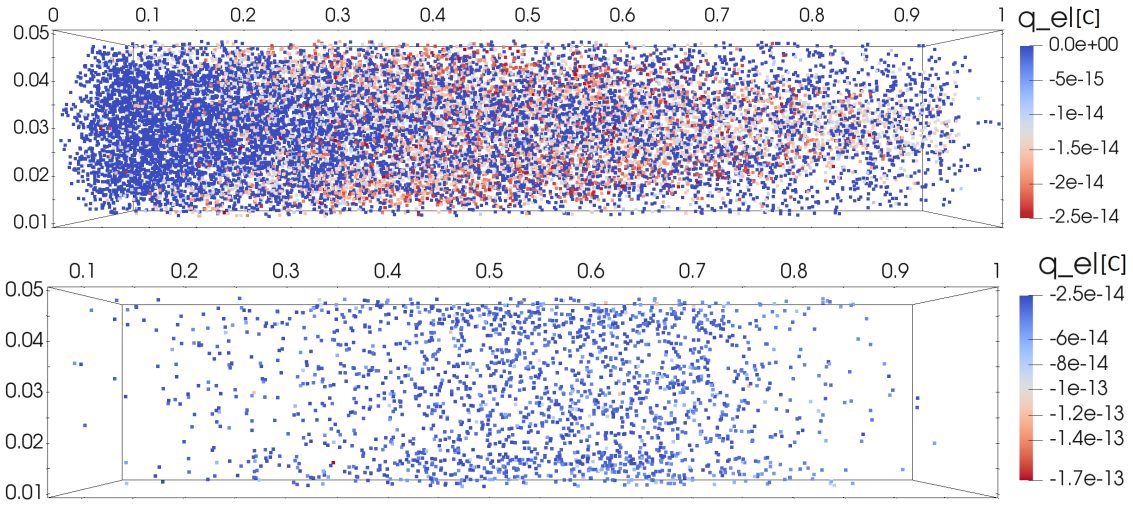

Figure 2.4: Snapshot of the pneumatic transport of PMMA powder through a steel pipe at t = 0.03 s in the axial direction. For better visualisation, the radial coordinate is scaled by a factor five.

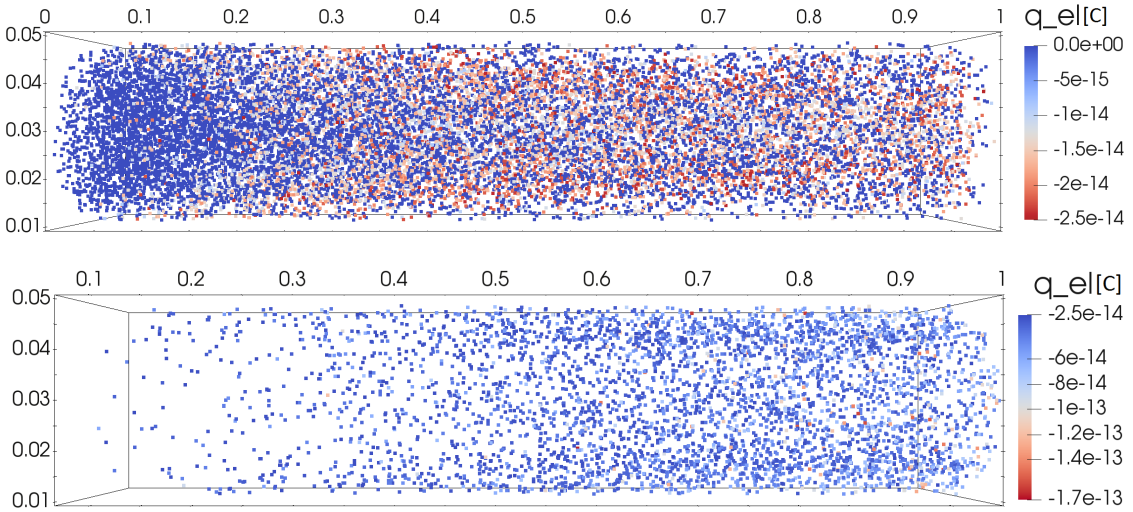

Figure 2.5: Snapshot of the pneumatic transport of PMMA powder through a steel pipe at t = 1 s in the axial direction. For better visualisation, the radial coordinate is scaled by a factor five.

The powder becomes more charged at the end of the pipe after the particles have impacted several times the wall. Figure 2.6 shows for the second time, t = 1s, the charges value per particles in the radial direction. It can be seen that heavily charged particles are more present near the pipe wall. This phenomenon is called turbophoresis : the particles have the tendency to migrate in the direction of decreasing turbulence level.

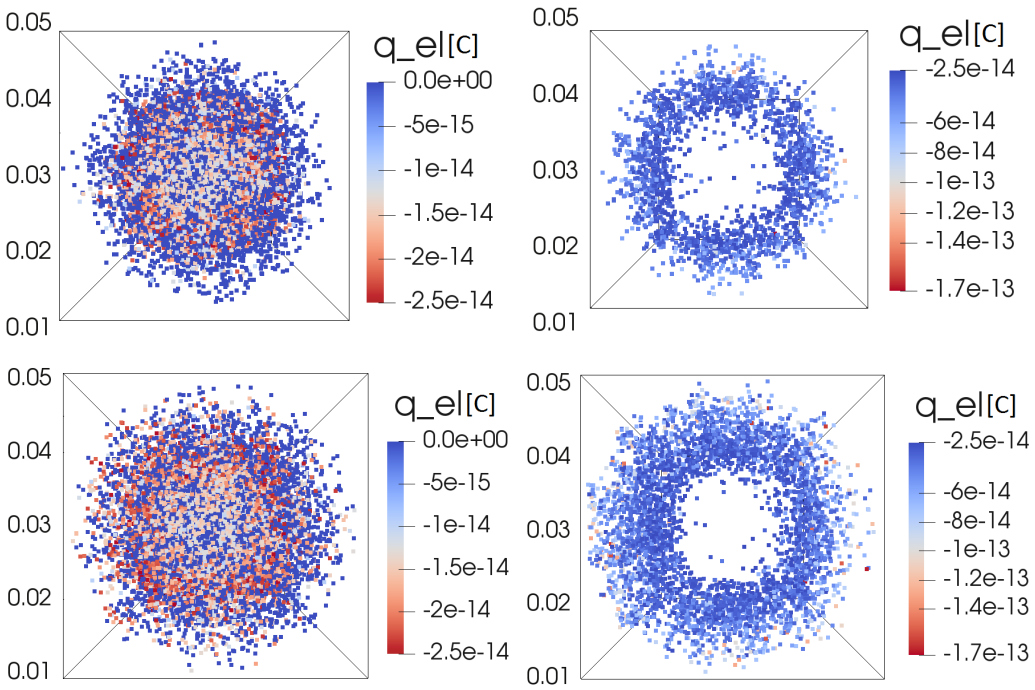

Figure 2.6: Snapshot of the pneumatic transport of PMMA powder through a steel pipe at t = 1 s in the radial direction.

Figures 2.7 and 2.8 show the distribution of particles velocities in the radial and axial direction respectively. As the fluid flow, the particles travel slower in the near wall region and the maximum value of velocity is at the centre of the pipe. For a fluid velocity of 30 m/s, we can see that in the centre region the particles travel faster with a gain of 50% compare to the inlet velocity.

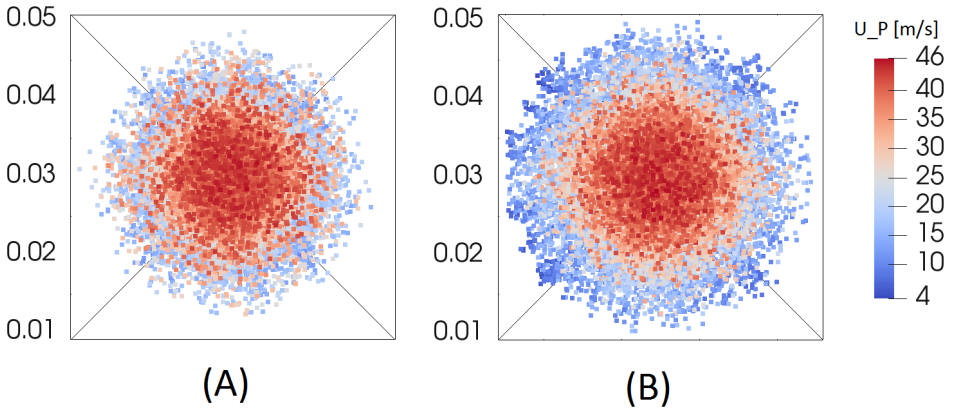

Figure 2.7: Snapshot of the pneumatic transport of PMMA powder through a steel pipe at (A) t = 0.03 s and (B) t = 1 s in the radial direction.

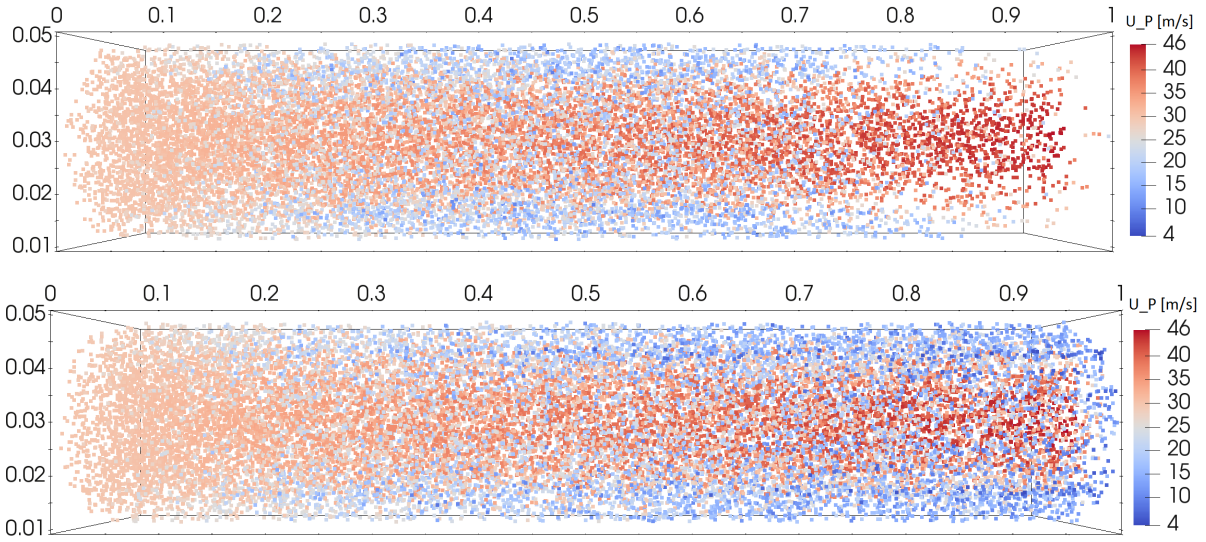

Figure 2.8: Snapshot of the pneumatic transport of PMMA powder through a steel pipe at t = 0.03 s and t = 1 s in the axial direction. For better visualisation, the radial coordinate is scaled by a factor five.

2.2 Effect of the particle diameter

The particles diameter has appear in all the equations of the charge exchange. We are interested in looking how the powder electrification is affected by this parameter. To this end, we have set three values for the diameter to make comparisons with the nominal case : 150, 600 and 1200 μm. The numbers of particles at the inlet are for each case **5 471 421** particles, **85 518** particles and **10 691** particles, respectively . As before, we will discussed the distribution of the electrical charges on the powder at the outlet first. Then, we will looked at the number of wall-collisions and how it affects the electrification. After that, the results from charge exchanges during the wall-impacts will be discussed.

For the simulations, we have made an assumption that is important to point out before analysing the results. By definition, the mass flow rate at the inlet of the pipe is given by the following equation :

$$\dot{m} = \frac{N\ V_p\ \rho}{\tau}, \tag{2.1}$$

where N is the number of particles, V_p is the volume of one single particle, ρ is the material density and τ is a time factor. The mass flow rate has been kept the same while letting vary the particle diameter. Then, Equation2.1 implies that the number of injected particles varies as we consider different diameters. More specifically, if the diameter changed by a factor k then the number of injected particles will significantly be impact by a factor k^{-3}.

2.2.1 Electrical charges on powder at the outlet

First, the results about the electrification of the powder at the outlet are given in the following tables : Table 2.4 for 150-μm-diameter, Table 2.5 for 600-μm-diameter and Table 2.6 for 1 200-μm-diameter.

	Number of particles	Percentage
Total number of particles found at the outlet	4 316 713	100 %
Particles carrying charges	2 416 995	55.99 %
Particles carrying no-charges	1 899 718	44.01 %
Charge range		
between -3 and -5e-2 [pC]	83 827	1.95 %
between -5e-2 and -5e-3 [pC]	329 965	7.65 %
between -5e-3 and -5e-4 [pC]	945 211	21.89 %
between -5e-4 and -5e-8 [pC]	41 518	0.96 %
between -5e-8 and -5e-12 [pC]	736 636	17.06 %
between -5e-12 and 0 [pC] (value of 0 exclude)	279 838	6.48 %
	Value	Units
Average value of the charges carried by the particles	-0.0039	pC
Absolute value of the maximum charge carried	2.75	pC

Table 2.4: Collected data for carried charges at the pipe outlet for PMMA powder of 150 μm diameter.

	Number of particles	Percentage
Total number of particles found at the outlet	59 186	100 %
Particles carrying charges	52 068	87.97 %
Particles carrying no-charges	7 118	12.03 %
Charge range		
between -3 and -0.5 [pC]	1 664	2.81 %
between -0.5 and -0.4 [pC]	2 860	4.83 %
between -0.4 and -0.3 [pC]	7 279	12.3 %
between -0.3 and -0.2 [pC]	12 009	20.29 %
between -0.2 and -0.1 [pC]	22 835	38.58 %
between -0.1 and 0 [pC] (value of 0 exclude)	5 421	9.16 %
	Value	Units
Average value of the charges carried by the particles	-0.1917	pC
Absolute value of the maximum charge carried	2.57	pC

Table 2.5: Collected data for carried charges at the pipe outlet for PMMA powder of 600 μm diameter.

	Number of particles	Percentage
Total number of particles found at the outlet	6 875	100 %
Particles carrying charges	6 299	91.62 %
Particles carrying no-charges	576	8.38 %
Charge range		
between -50 and -3 [pC]	460	6.69 %
between -3 and -2 [pC]	2 226	32.38 %
between -2 and -1 [pC]	3 071	44.67 %
between -1 and 0 [pC] (value of 0 exclude)	542	7.88 %
	Value	Units
Average value of the charges carried by the particles	-1.7964	pC
Absolute value of the maximum charge carried	46	pC

Table 2.6: Collected data for carried charges at the pipe outlet for PMMA powder of 1 200 μm diameter.

Theses tables show at first the quantity of powder leaving the pipe and its percentage electrically charged. After that, the partition on different intervals of charge value is presented. Finally, the average and maximum values of charge are shown.

The first observation is that the percentage of particles carrying charges increases with the diameter. Only a little more than half of the powder is electrically charged for the case of the smallest diameter while, for the case of the largest diameter, the percentage is more than 90 %.

A second observation is that the average charge increases by an order of magnitude when the diameter decreases by two. The charge exchange equations are reminded here :

(i) during wall-collision :

$$\Delta Q_c = CV_c\,(1 - exp(-\Delta t_{pw}/\tau_w)) \propto R^2|u_p^{4/5}|\left(1 - exp(-a_1 R|u_p^{-1/5}|)\right),$$

(ii) during inter-particles collision :

$$\Delta Q_1 = \frac{C_1 C_2}{C_1 + C_2}(\frac{Q_2}{C_2} - \frac{Q_1}{C_1})(1 - exp(-\Delta t_p/\tau_p)) \propto \Delta Q\left(1 - exp(-a_2 R|u_{12}^{3/5}|)\right),$$

with a_1 and a_2, two constants. In both equations, we can observe that the exponents involve the particle diameter. Since the sizes of the particles are very small, this have a direct consequence on the exchanges. The higher the diameter is, the higher the charge exchange becomes. Also for the contact electrification with the wall, the transfers depend on the square of the diameter, which also leads to higher charges exchanges. Because of these factors, the particles gain smaller charges during wall-collisions and the exchange during inter-particle collisions will be even lowered.

All theses results are illustrated in Figures 2.9, 2.10 and 2.11 below. Each graphs displays two parts as the nominal case : one resulting from the interactions with the wall on the left and a region containing very small values of charges or zero charge on the right. This second region comes only from inter-particles collisions. On the graphs, we can seen that the mechanism of

inter-particles exchanges seems more important for the case of the smallest diameter. Because more particles are injected, the probability to hit an other particle is higher in this case and can explain why this percentage increases.

Because the range is wide, these distributions show more than 90 % of the powder but do not display the extreme values on the left of the graphs. The absolute value of maximum charge carried can be found in the last section of each tables above. For the case of the 150 μm diameter, the maximum value is very high compare to the average charge, around 700 times more. For others diameter variations, the ratio is between 150 and 15 depending on the case. As it will be shown in the next section, this difference comes from the maximum number of collisions and the percentage of particles undergoing more than two impacts with the wall. At each impact, the particles gain some electrical charges on their surfaces. In the case of the smallest diameter, more particles undergo several impacts with the wall and then the maximum charge value reaches also higher value.

The shape of each figures depicts the same behaviour with the peak in the range of higher values found between -0.003 and -0.001 for the case of the 150 μm diameter, between -0.03 and -0.01 for the case of the 300 μm diameter between -0.3 and -0.1 for the case of the 600 μm diameter, between -3 and -1 for the case of the 1 200 μm diameter. The range grows with the diameter and this variation arises from the particles velocity as it can be seen on the previous equations. The particles can accelerate or decelerate during inter-particle collisions and will always decelerate during wall collision. With higher velocity, the contact leads to higher electrical exchange charge with the wall.

Finally, for the larger diameter size, the peak of the distribution do not appear clearly ; the distribution is more or less uniformly distributed between -2.5 and -1 pC.

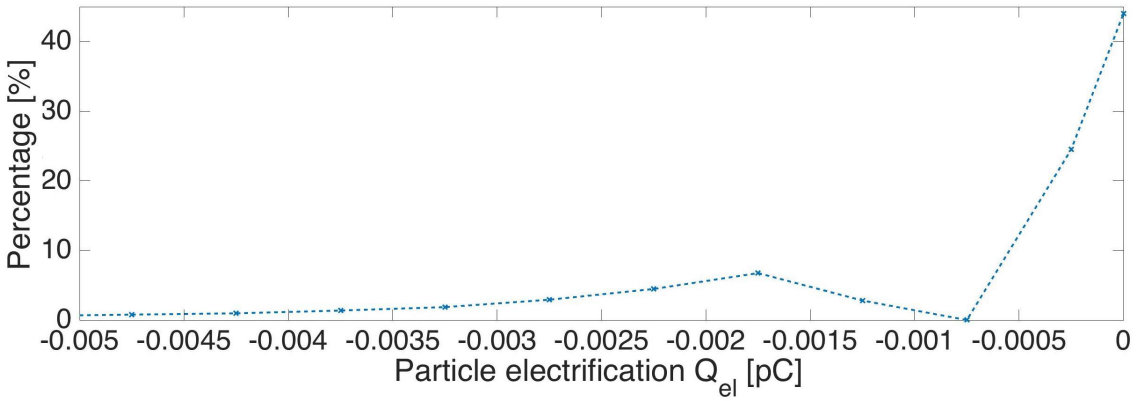

Figure 2.9: Distribution of particle electrification for PMMA powder of 150 μm. The x-axis corresponds to the electric charge. The y-axis corresponds to the percentage of particles carrying a given charge.

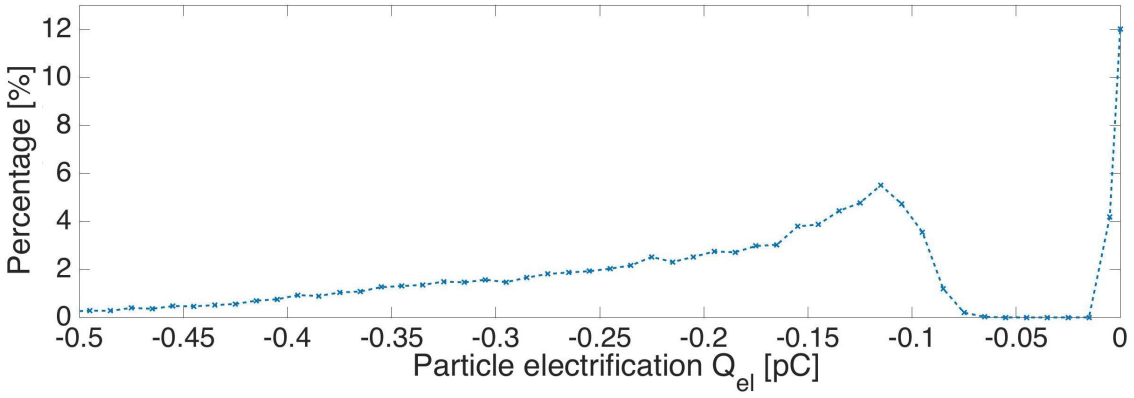

Figure 2.10: Distribution of particle electrification for PMMA powder of 600 μm. The x-axis corresponds to the electric charge. The y-axis corresponds to the percentage of particles carrying a given charge.

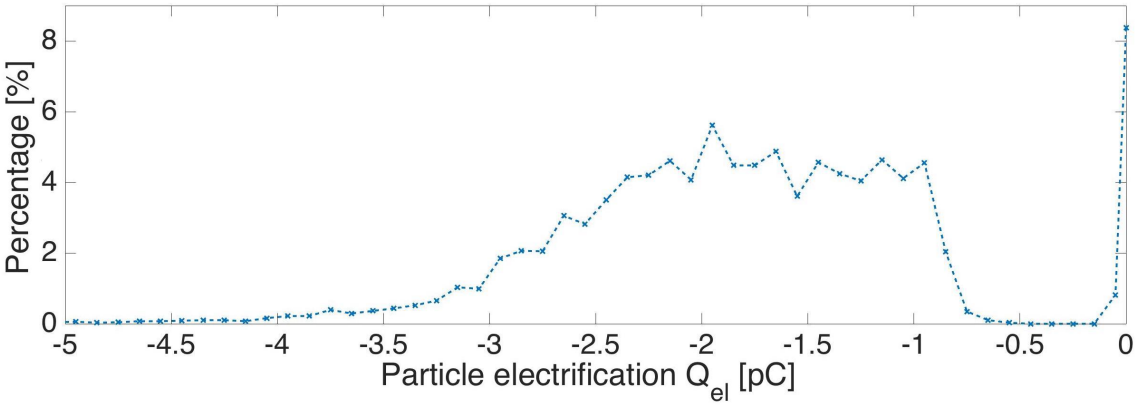

Figure 2.11: Distribution of particle electrification for PMMA powder of 1 200 μm. The x-axis corresponds to the electric charge. The y-axis corresponds to the percentage of particles carrying a given charge.

2.2.2 Effect of the particle diameter on the number of collisions with the wall

Tables 2.7, 2.8 and 2.9 below show the number of collisions occurring with the pipe and the percentages of particles undergoing theses collisions. The second part of the tables shows data for the particles that did not collide at all with the wall. We can see the percentage of them leaving the pipe electrically charged because of inter-particle collisions. This percentage is based on the whole powder. The average and maximum charge exchange for this mechanism are also presented.

It can be seen that the number of particles undergoing no collision increases by a factor two when the diameter decreases by the same factor. In each cases, the majority of particles will only collide one time with the wall. For the case of the biggest diameter, the percentage of particles undergoing two impacts is nearly as important than the percentage of one collision.

Number of wall collision	Number of particles	Percentage
0 collision	2 957 710	68.52 %
1 collision	1 004 956	23.28 %
2 collisions	124 240	2.88 %
3 collisions	39 528	0.92 %
more than 4 collisions	190 279	4.4 %
Maximum number of collisions	81	-
Particles undergoing no collision	Value	Units
Percentage of particles carrying charges	24.51 %	-
Average value of the charges carried	-3.4958e-8	pC
Absolute value of the maximum charge carried	4.16e-4	pC

Table 2.7: Collected data for the numbers of collisions at the pipe outlet for PMMA powder of 150 μm diameter.

Number of wall collision	Number of particles	Percentage
0 collision	9 601	16.22 %
1 collision	37 406	63.2 %
2 collisions	11 124	18.8 %
3 collisions	1 014	1.71 %
more than 4 collisions	41	0.07 %
Maximum number of collisions	5	-
Particles undergoing no collision	Value	Units
Percentage of particles carrying charges	4.2 %	-
Average value of the charges carried	-4.0916e-6	pC
Absolute value of the maximum charge carried	5.16e-4	pC

Table 2.8: Collected data for the numbers of collisions at the pipe outlet for PMMA powder of 600 μm diameter.

We can also notice the decrease of the maximum number of collisions when increasing the diameter : for the case of 1 200 μm diameter, at most four collisions will occur while in the case of 150 μm diameter the maximum number of collisions is 81. The electrical charges of the powder come from the collisions with the wall. When the particles are already charged, the exchange during impact will be lowered but it still gives an increase of electrical charge. Because the maximum number of collision is very high for the case of the smallest diameter, some particles can be heavily charged, which explain why the extend of transport charge is so large. In the same manner, the percentage of particles undergoing more than four collisions is much higher, nearly 5 %, for the case of the smallest diameter against less than 1 % in all others cases.

Number of wall collision	Number of particles	Percentage
0 collision	632	9.19 %
1 collision	3 309	48.13 %
2 collisions	2 606	37.91 %
3 collisions	314	4.57 %
4 collisions	14	0.2 %
Maximum number of collisions	4	-
Particles undergoing no collision	Value	Units
Percentage of particles carrying charges	0.82 %	-
Average value of the charges carried	-4.6706e-5	pC
Absolute value of the maximum charge carried	6.04e-4	pC

Table 2.9: Collected data for the numbers of collisions at the pipe outlet for PMMA powder of 1 200 μm diameter.

As mentioned in the previous results, less particles will leave the pipe carrying charge when the diameter size is smaller. On the other hand, when looking at the results of inter-particle collisions, in the case of the smallest diameter, the powder is more sensitive to this mechanism. Nearly 25 % of the powder will gain electrical charges in this manner. This percentage decreases to reach less than 1 % for the case of the highest diameter value. This is because of the difference at the number of injected particles : when this number is higher, the probability to hit an other particle is also higher. The magnitude of charge exchange during inter-particle collisions does not depend on the square of the diameter as it is the case for the exchange with the wall but it depends on the difference of charge over the particles. Since the value is smaller of an order of magnitude, it will impact also this exchange that will be reduce by a factor ten when decreasing the diameter.

Figures 2.12, 2.13 and 2.14 illustrate the charge exchange increase and accumulated charge exchange during wall-collisions. A general trend is that the accumulated charge tends to reach an equilibrium after several impacts. For the cases of 600 and 1 200 μm diameter, this equilibrium is reached after two collisions because only a small part of the powder will collide more than two times with the wall. This will only slightly increase the overall charge of the powder. For the case of 150 μm diameter, this equilibrium is reached after 25 collisions. Only one third of the powder have impacted the wall and 4.4% of it had undergo more than three impacts. We can see in Figure 2.12 that the charge exchange increase for one collision is the higher contribution to the accumulated charge exchange. This comes from the percentage of particles undergoing only one impact with the wall that is the larger. At higher number of collision, the accumulated charge exchange continues to growth slowly until reaching the plateau at $n_{wc} = 25$ collisions. The inter-particle charge exchanges do not increase the overall charge of the powder but can reduce the charge of one particle between two impacts. Due to that, the following charge exchange with the wall can be slightly higher.

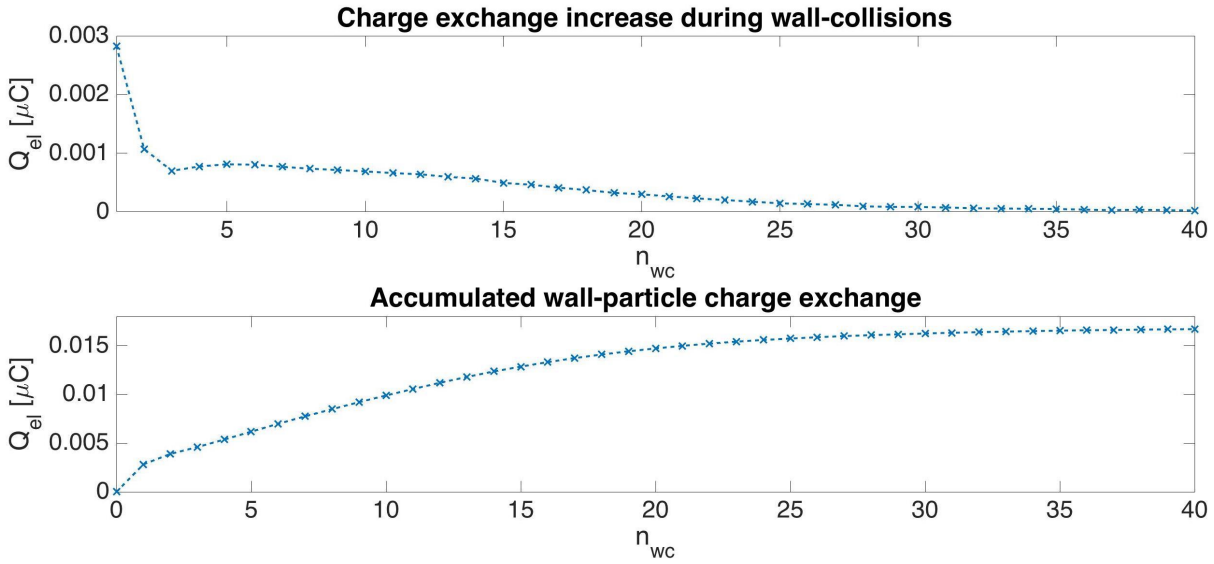

Figure 2.12: Charge exchange increase and accumulated charge exchange during wall-collisions for 150 μm diameter particles : the accumulated charge at n_{wc} = i is the addition of the accumulated charge at n_{wc} = i-1 and the charge exchange increase at n_{wc} = i.

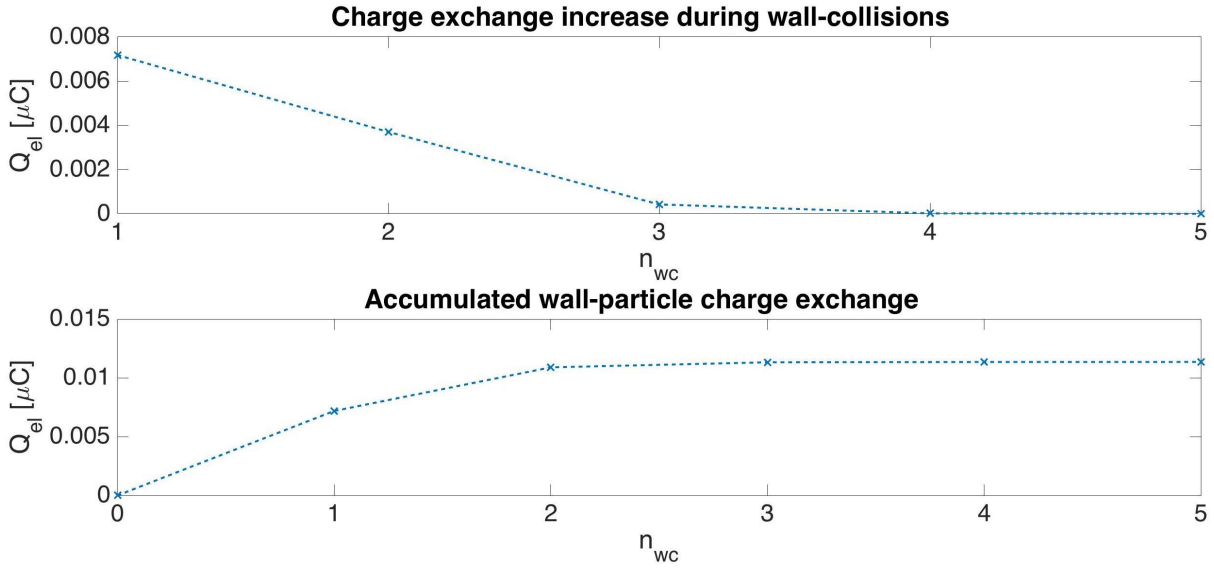

Figure 2.13: Charge exchange increase and accumulated charge exchange during wall-collisions for 600 μm diameter particles : the accumulated charge at n_{wc} = i is the addition of the accumulated charge at n_{wc} = i-1 and the charge exchange increase at n_{wc} = i.

According to Figure 2.14, in the case of 1 200 μm diameter, the behaviour is different. The gain at the second collision is nearly the same as the first one. At first, we can notice that the percentage of particles undergoing a second collision is more important in this case. The exchange depends also on the values of contact surface and the velocity of the particle. When the diameter increases, the contact surface also increases. Because of that, the charge exchange increase due to a second collision can be higher in this case.

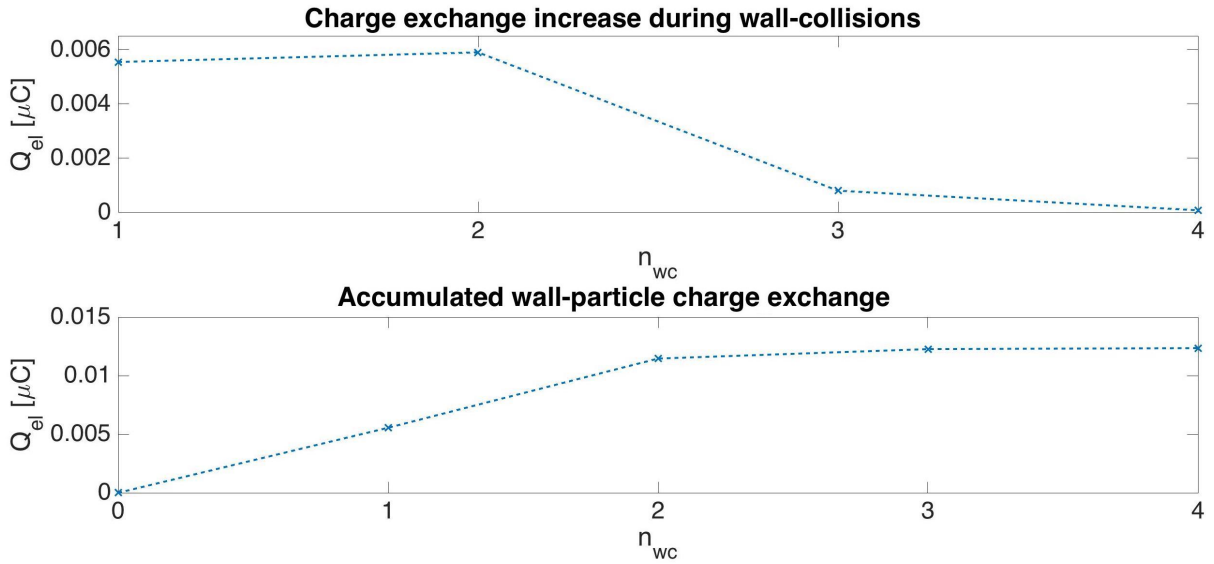

Figure 2.14: Charge exchange increase and accumulated charge exchange during wall-collisions for 1 200 μm diameter particles : the accumulated charge at n_{wc} = i is the addition of the accumulated charge at n_{wc} = i-1 and the charge exchange increase at n_{wc} = i.

At the end, Figure 2.15 summarises for all diameter variations the charge exchange increase and accumulated charge exchange during wall-collisions. At first, the behaviour of the case of the smallest diameter is different and the accumulated charge tends to a higher value than the others. For the three others cases, the plateau is reach more faster and the case of the largest diameter seems to accumulated higher magnitude of charge

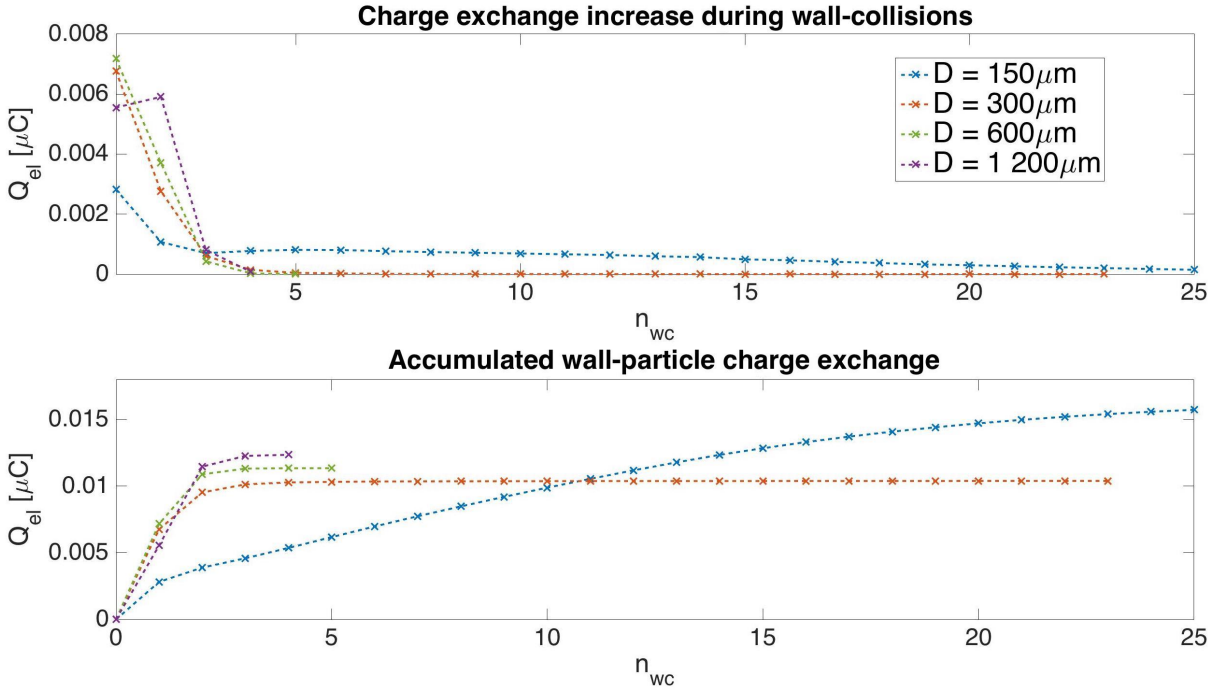

Figure 2.15: Charge exchange increase and accumulated charge exchange during wall-collisions for different diameters : the accumulated charge at n_{wc} = i is the addition of the accumulated charge at n_{wc} = i-1 and the charge exchange increase at n_{wc} = i.

To provide a better comparison, these graphs have been normalised using the total surface of the

powder, which is equal to the number of particles multiplied by the surface of one particle. The total volume of the powder had been keep constant for each case but the total surface available for electrification is different. The 150-μm-diameter powder has a surface that is two times larger than the one of the powder of the nominal case. The 600- and 1 200-μm-diameter powder are two times and four times smaller, respectively. Based on this normalisation, the comparison can be seen in Figure 2.16.

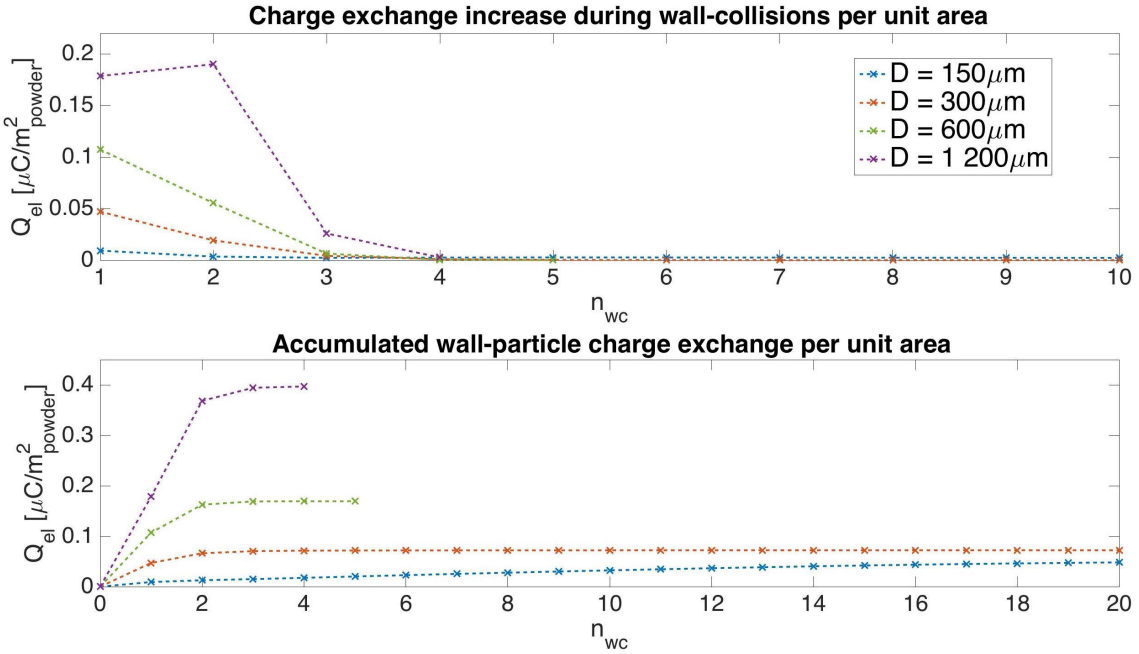

Figure 2.16: Normalisation of the charge exchange increase and accumulated charge exchange during wall-collisions for different diameters : the accumulated charge at n_{wc} = i is the addition of the accumulated charge at n_{wc} = i-1 and the charge exchange increase at n_{wc} = i.

Since the electrical capacity depends on the diameter, the smallest one can carried less charges than the others. The plateau values with the normalisation are summarised in the table below for each particle diameter. The last column represent the plateau value in each case divided by the value reaches by the nominal case. A constant ratio appears for higher diameter variation.

Diameter	$Q_{el,pl}$ [μC/m^2]	$Q_{el,pl}/Q_{el,pl}^{Nom}$ [-]
150 μm	0.0554	$0.766 = \frac{1}{1.3}$
300 μm	0.0723	1
600 μm	0.1695	2.344
1 200 μm	0.3971	$5.492 \approx 2.34^2$

2.2.3 Magnitude of the charge exchange during wall collisions

In this last section of our parametric study with respect to the diameter, the charge exchanges during wall collisions will be analyzed. The results for the different simulations are summarised in Tables 2.10, 2.11 and 2.12 for the powders of 150, 600 and 1 200 μm diameter, respectively. Theses tables give the number of collisions occurring during the simulation and the subdivision of the charges exchanges range with percentage of impacts belonging in these ranges.

	Number of collisions	Percentage
Total number of collisions with the wall	5 481 128	100 %
Charge range		
between -0.01 and 0 [pC]	332	0.006 %
between 0 and 0.0025 [pC]	1 787 305	32.61 %
between 0.0025 and 0.005 [pC]	2 169 039	39.57 %
between 0.005 and 0.0075 [pC]	778 198	14.2 %
between 0.0075 and 0.01 [pC]	353 147	6.44 %
between 0.01 and 0.75 [pC]	393 107	7.17 %

Table 2.10: Collected data for charge exchanges during wall collisions for PMMA powder of 150 μm diameter.

	Number of collisions	Percentage
Total number of collisions with the wall	117 013	100 %
Charge range		
between 0 and 0.1 [pC]	22 575	19.29 %
between 0.1 and 0.15 [pC]	42 108	35.99 %
between 0.15 and 0.2 [pC]	22 518	19.24 %
between 0.2 and 0.25 [pC]	12 456	10.65 %
between 0.25 and 0.5 [pC]	16 153	13.8 %
between 0.5 and 5 [pC]	1 203	1.03 %

Table 2.11: Collected data for charge exchanges during wall collisions for PMMA powder of 600 μm diameter.

A first observation is the appearance of negative charge exchanges for the 150-μm-diameter powder containing 332 collisions. This means that some particles have given electron(s) to the pipe material supposing that they were heavily charged before the collisions. For this sample, the number of particles undergoing more than four collisions is near 5 % when in others cases, it represents less than 1 %. As it was seen in the previous section, these particles carry larger amount of charge. They can reach at the end values that are three orders of magnitude more important than the average charge.

	Number of collisions	Percentage
Total number of collisions with the wall	17 952	100 %
Charge range		
between 0 and 0.75 [pC]	2 859	15.93 %
between 0.75 and 1 [pC]	5 480	30.53 %
between 1 and 1.5 [pC]	5 933	33.05 %
between 1.5 and 2.5 [pC]	3 014	16.79 %
between 2.5 and 5 [pC]	595	3.31 %
between 5 and 30 [pC]	71	0.4 %

Table 2.12: Collected data for charge exchanges during wall collisions for PMMA powder of 1 200 μm diameter.

This means that in the equation for charge exchange with the wall :

$$\Delta Q = \Delta Q_c + \Delta Q_t, \tag{2.2}$$

the term of transfer due to pre-charge became higher than the term of contact.

In Table 2.13, it can be observed as before that the average charge exchange decreases by one order of magnitude when the diameter decreases by a factor two. About the contact time with the wall, the average value for the case of the smallest diameter is higher than the cases of 600 μm and 1 200 μm diameter. This comes from the maximum time that is larger for this diameter size. All the cases are made of the same powder and have the same mechanical properties. This means that the differences between the examined cases can only occur via the variation of diameter of the particles or their velocity. Based on Equation 1.29, we know that the contact time increased when the particle velocity decreases but, on the other hand, the contact area becomes smaller.

	150 μm	600 μm	1 200 μm	Units
Average value of the charges exchanges	0.0046	0.1694	1.2232	pC
Average area of contact	0.5736	16.569	70.627	nm^2
Average time of contact	50.573	42.858	70.955	μs
Minimum value of the charges exchanges	-0.0099	0.064	0.509	pC
Minimum area of contact	0.195	4.97	35.3	nm^2
Minimum time of contact	3.44	14.2	27.9	μs
Maximum value of the charges exchanges	0.7110	2.43	25.8	pC
Maximum area of contact	1.15	19.7	79.6	nm^2
Maximum time of contact	13.1	0.936	2.6	ms

Table 2.13: Average, minimum and maximum values of charge exchange, contact area and contact time during wall-collisions as function of the particle diameter.

Figures 2.17, 2.18 and 2.19 show the distributions of charge exchange for the different diameters. These distributions have the same shape but the peak values have different percentages. This is because of the wide of the range. For 150 μm diameter, more than 7 % of collisions will result to exchanges higher than 0.01 pC while for the two other cases, this percentage is lower than 1 % and is not depicted in the graph.

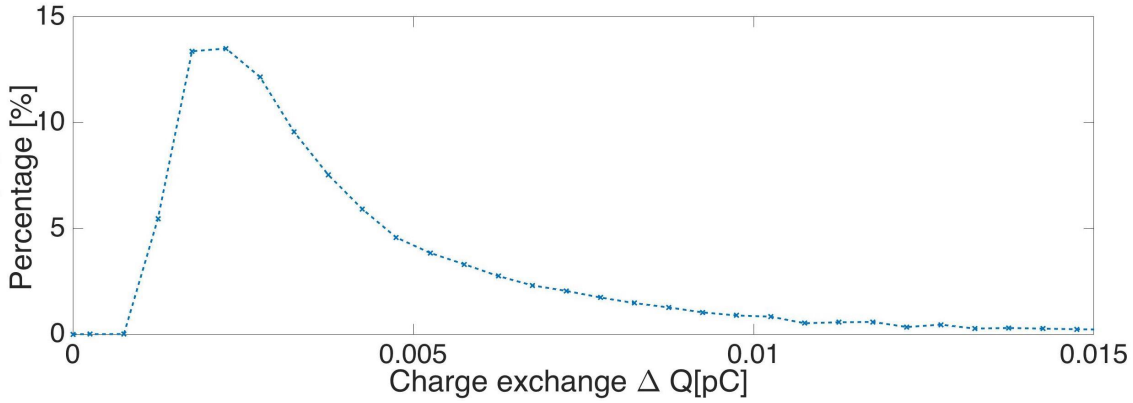

Figure 2.17: Distribution of charge exchange during wall-collisions for PMMA powder of 150 μm. The x-axis corresponds to the electric charge. The y-axis corresponds to the percentage of collisions exchanging a given charge.

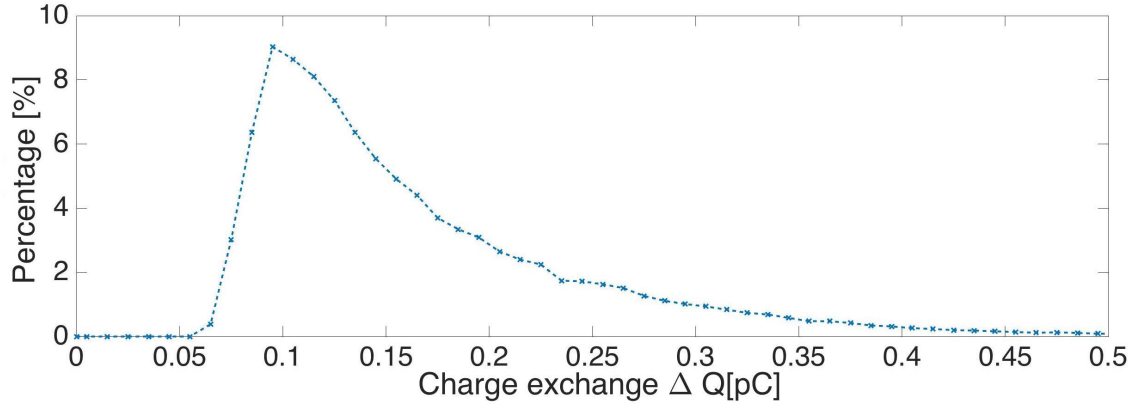

Figure 2.18: Distribution of charge exchange during wall-collisions for PMMA powder of 600 μm. The x-axis corresponds to the electric charge. The y-axis corresponds to the percentage of collisions exchanging a given charge.

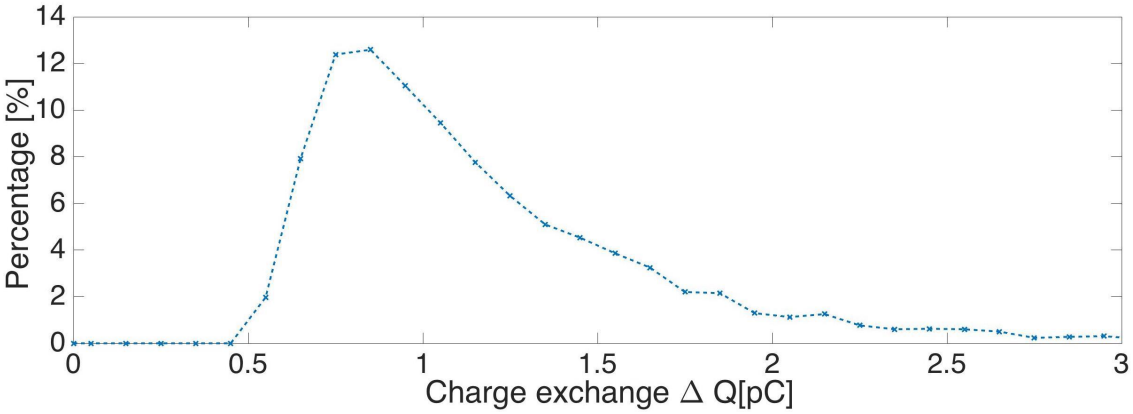

Figure 2.19: Distribution of charge exchange during wall-collisions for PMMA powder of 1 200 μm. The x-axis corresponds to the electric charge. The y-axis corresponds to the percentage of collisions exchanging a given charge.

2.3 Parametric study with respect to mass flow rate

In this section, we discuss how the mass flow rate of particles impacts the electrification of the powder. To this end, we have simulated flows with different mass flow rates and compared them

to the nominal case. In these simulations, the diameter is fixed at 300 μm and the mass flow rates are set at 5 and 50 g/s. The quantities injected at the inlet of the pipe are **342 093** and **3 418 426** particles, respectively.

The description of the results will follow the same structure as in the previous section. At first, a description from carried charges at the outlet will be given. Subsequently, the number of wall collisions and the effect of inter-particle collisions will be discussed. Finally, the results for the charge exchange during wall-collisions will be presented.

2.3.1 Electrical charge of the powder at the outlet and number of collisions with the wall

Table 2.14 summarises the electrical charges found on the particles at the outlet of the pipe and the number of collisions these particles undergo with the wall. The first observation is the decrease of the percentage of particles carrying charges when the mass flow rate is reduced. Nearly 25 % of the powder is not electrically charged when the mass flow rate of particle is small against 6% for the highest mass flow rate.

The ranges of charging are of the same order of magnitude for all case. Nevertheless, some variations occur in the percentages of the range subdivision. These variations can be more easily seen in Figure 2.20 that depicts the percentages of carried charge for each mass flow rate values. The major difference is the percentage of smallest charge values when the mass flow rate is larger : 40% of the powder against less than 10% for the lowest mass flow rate. This comes from the interactions between particles. When the mass flow rate is higher, the probability of two particles impacting each other is higher. These impacts only redistribute the charges on the powder and the exchange is small compared to the exchanges due to wall collisions. Upon observation of the last section of the table about the percentage of particles undergoing no collision, it can be seen that the percentage of small charges carried correspond exactly to the percentage of particles charged due to inter-particle collisions : 8.55 % and 39.52 % for the mass flow rate equal to 5 and 50 g/s, respectively.

The third section of the table gives information about the number of collisions undergoing by the particles. Although the percentage of particles undergoing no collision increases with the mass flow rate, the percentage of particles undergoing at least two collisions is also higher. 17.41% of the powder has multiple impacts with the wall for the case of the highest mass flow rate against 9.16% for the case of the lowest one. For the larger mass flow rate, the assumption of dilute transport regime is not anymore valid and we can no longer assume that the particles are not affected by their neighbouring particles. They can impact more often the others particles.

	$\dot{m}$ = 50 g/s		$\dot{m}$ = 5 g/s	
	Number of particles	Percentage	Number of particles	Percentage
Total number of particles found at the outlet	2 532 352	100 %	253 769	100 %
Particles carrying charges	2 375 525	93.81 %	196 247	77.33 %
Particles carrying no-charges	156 827	6.19 %	57 522	22.67 %
Charge range				
between -11 and -0.05 [pC]	322 828	12.75 %	22 010	8.67 %
between -0.05 and -0.025 [pC]	365 023	14.41 %	52 394	20.65 %
between -0.025 and -0.005 [pC]	686 906	27.13 %	100 150	39.46 %
between -0.005 and 0 [pC] (value between 0 exclude)	1 000 768	39.52 %	21 693	8.55 %
Number of wall collision				
0 collision	1 157 595	45.71 %	79 215	31.22 %
1 collision	933 636	36.87 %	151 289	59.62 %
2 collisions	313 400	12.38 %	20 606	8.12 %
3 collisions	94 123	3.72 %	2 081	0.82 %
more than 4 collisions	33 598	1.32 %	578	0.22 %
Maximum number of collisions	50	-	37	-
	Value	Units	Value	Units
Average value of the charges carried by the particles	-0.0208	pC	-0.0203	pC
Absolute value of the maximum charge carried	10.5	pC	4.53	pC
Particles undergoing no collision	Value	Units	Value	Units
Percentage of particles carrying charges	39.52 %	-	8.55 %	-
Average value of the charges carried	-2.8483e-7	pC	-2.2405e-7	pC
Absolute value of the maximum charge carried	8.76e-4	pC	9.76e-5	pC

Table 2.14: Collected data about carried charges and the number of collisions at the pipe outlet for the mass flow rates variations.

Because of that, a particle can impact the wall, then another particle and go back against the wall. This can explain why more particles have impacted several times the wall and the increase of the maximum number of collision with the wall for the case of the larger mass flow rate. It can also explain the higher percentage of particles that do not interacted with the wall. The particles at the centre of the pipe will collide between them and the majority will stay in the centre.

The powder gains its electrical charge because of impacts with the wall. When one particle impact several times, the gain at each collision decreases because of the charge on the surface but it's still give an addition to the particle charge. As a result in the fourth part of the table, the maximal charge carried by particles is around two times higher for the larger mass flow rate. On the other hand, the average value is nearly the same for all the values of the mass flow rate variations, around -0.02 pC. Even if fewer particles interact with the wall, the total number of collisions increases by the same factor as the mass flow rate, as it will be seen in the next section. At the end, with a higher mass flow rate, the percentage of particles having interactions with the wall is smaller. On the other hand, the percentage of particles with multiple wall-collisions is higher and, because of that, more particles are heavily charged at the outlet. This combination leads at the end to the same average value.

We can seen on the graph a drop in the percentage between -0.01 and -0.005 pC. Fewer particles have carried a charge in this interval. This region is the boundary between the two exchange mechanism : the higher magnitudes of charge comes from wall-collisions and the smaller magnitudes of charge comes from inter-particle collisions.

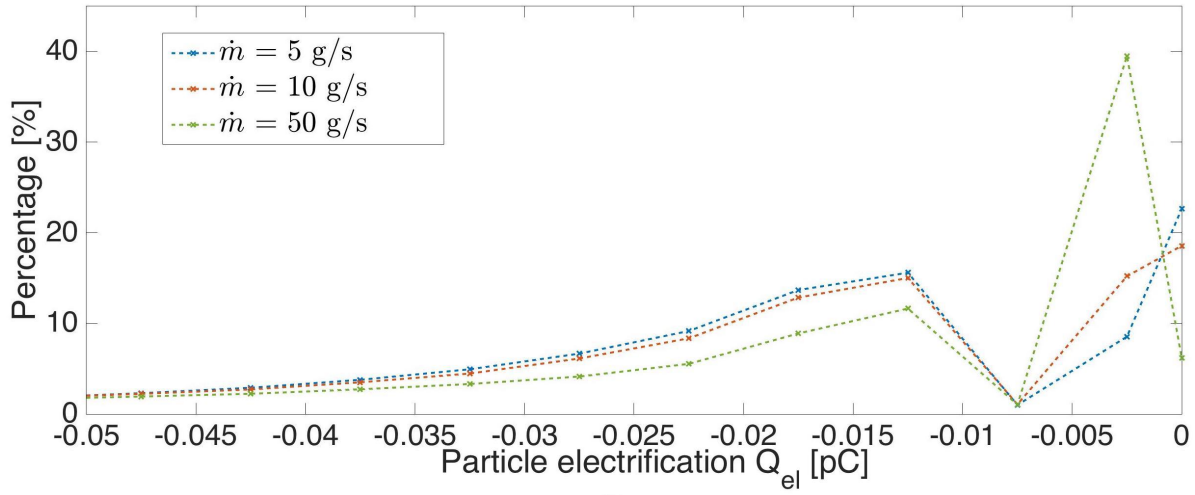

Figure 2.20: Distribution of particle electrification. The x-axis corresponds to the electric charge. The y-axis corresponds to the percentage of particles carrying a given charge.

This last point is illustrated in Figure 2.21 that shows the charge exchange increase and accumulated charge exchange during wall-collisions. It can be seen that higher the mass flow rate is, and higher the accumulated charge on the powder gets. This is because at higher mass flow rate, more particles are injected and a larger surface is available for the electrification. As before, an equilibrium plateau is reach after several collisions. The mass flow rates of 5 and 10 g/s depict the same trends whereas for the larger mass flow rate, this equilibrium is reached after a higher

number of collision because of the higher number of particles undergoing more than two impacts.

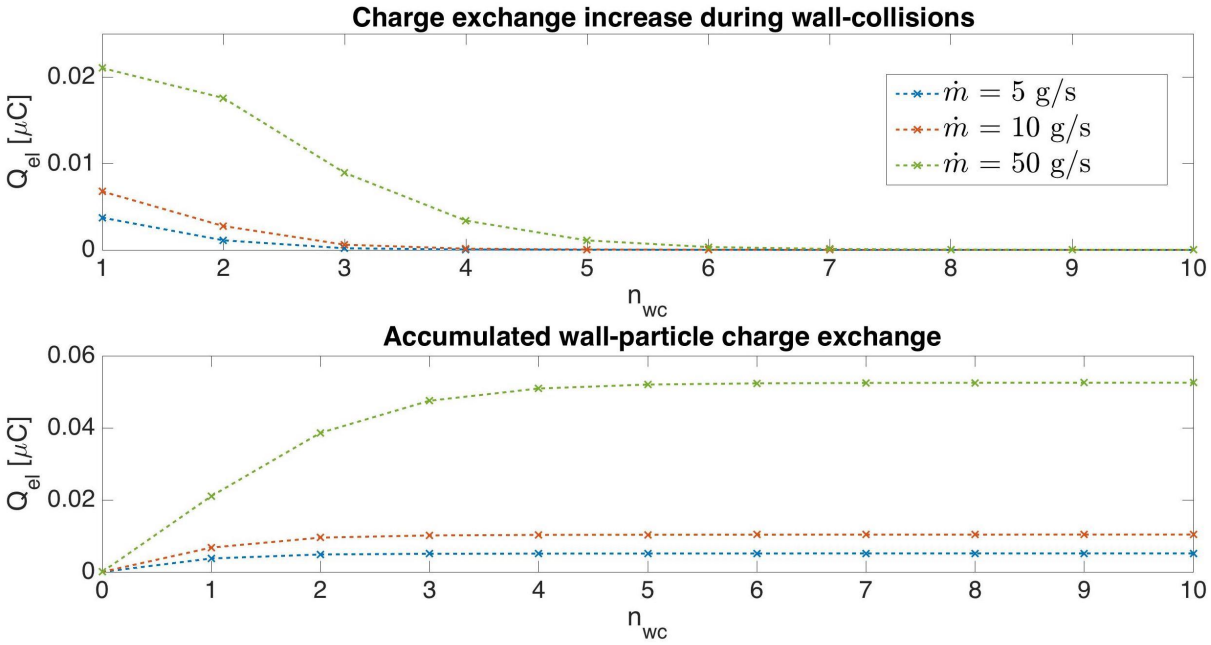

Figure 2.21: Charge exchange increase and accumulated charge exchange during wall-collisions for different mass flow rates : the accumulated charge at n_{wc} = i is the addition of the accumulated charge at n_{wc} = i-1 and the charge exchange increase at n_{wc} = i.

In order to provide a clearer comparison, the same normalisation using the total surface of the powder have been applied and the results are illustrated in Figure 2.22 below.

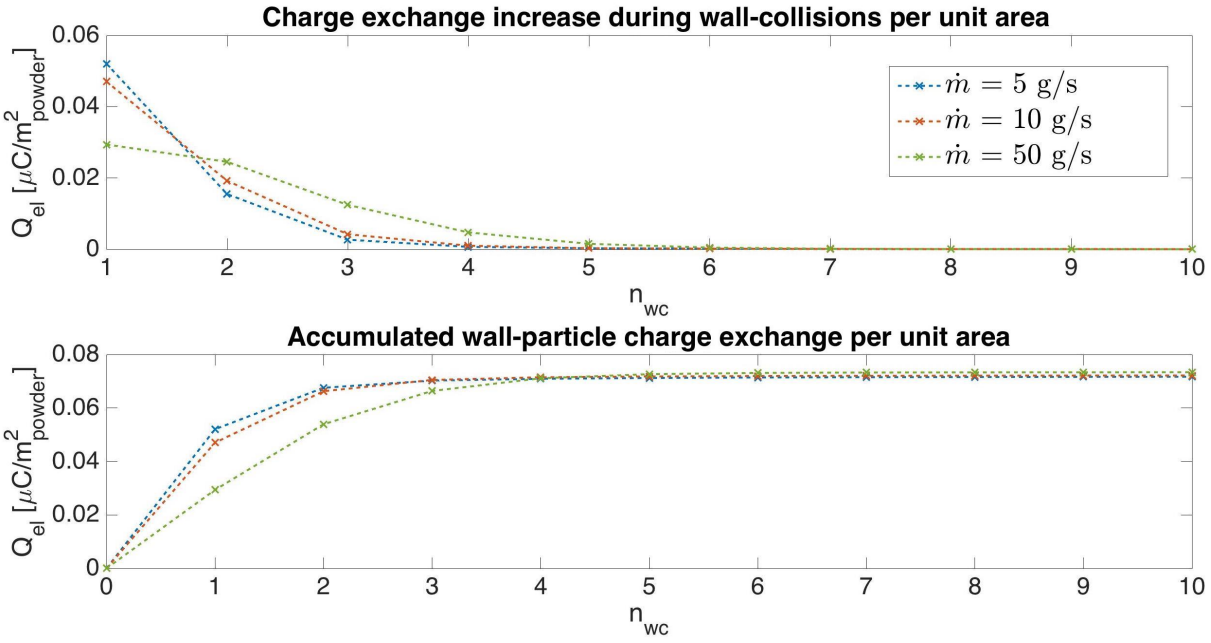

Figure 2.22: Normalisation of the charge exchange increase and accumulated charge exchange during wall-collisions for different mass flow rates : the accumulated charge at n_{wc} = i is the addition of the accumulated charge at n_{wc} = i-1 and the charge exchange increase at n_{wc} = i.

The three simulations tend to the same plateau value meaning that the mass flow rate does not impact the accumulation of charge over one particle. On the graph, it can be clearly seen that

the gained charge at the first impact is less important for the highest mass flow rate but the fact that the percentage of particles undergoing more impact is higher, the charge exchange increase is still important for $n_{wc} = 2$ and 3. At the end, the accumulated charge reaches the plateau only at $n_{wc} = 5$.

2.3.2 Magnitude of the charge exchange during wall collisions

The results for the charge exchange during wall-collisions can be found in Table 2.15. The first line of the table shows the total number of collisions and we can see that it has been increased by the same factor as the mass flow rate ratio. These results are also illustrated in Figure 2.23. It can be seen that the mass flow rate do not affect the exchange during wall contact and the curves show exactly the same profile with nearly the same percentages.

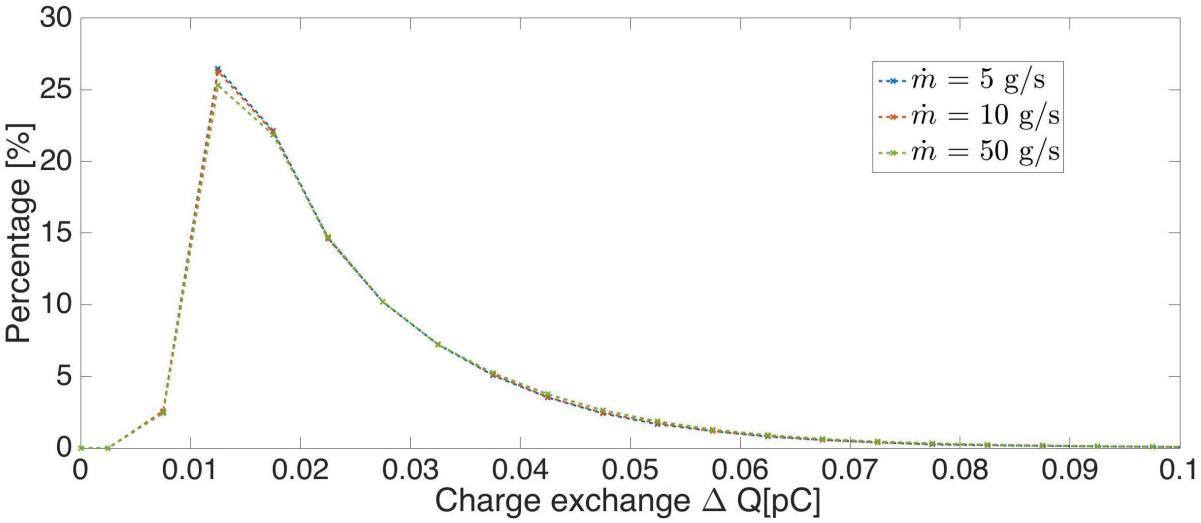

Figure 2.23: Distribution of charge exchange during wall-collisions for different mass flow rates. The x-axis corresponds to the electric charge. The y-axis corresponds to the percentage of collisions exchanging a given charge.

The only difference is the peak that is reduced by 1% for the case of the highest mass flow rate. This comes from the slightly larger percentage of higher magnitude of charge exchange. In the case of the higher mass flow rate, 13 % of collisions gives a charge exchange higher than 0.04 pC against 11.7 % for the case of the smallest one. Also, it can be seen in the last section of the table, the maximum and minimum contact time increases or decreases respectively with the mass flow rate. The charge exchange depends mainly on the mechanical properties of the powder and the wall and the particle velocities. Since in these simulations, we considered the same powder, the difference in the results are due to different particle velocities. Because of multiple impacts and the remove of dilute regime assumption for the larger mass flow rate, some particles can have the radial component of the velocity much smaller in absolute value than the two other simulations. This will increase the time of contact and at the end gives also a little bit larger exchange of charge.

	$\dot{m} = 0.05$ kg/s		$\dot{m} = 0.005$ kg/s	
	Number of collisions	Percentage	Number of collisions	Percentage
Total number of collisions with the wall	3 820 171	100 %	371 106	100 %
Charge range				
between 0 and 0.01 [pC]	93 163	2.44 %	9 318	2.51 %
between 0.01 and 0.02 [pC]	1 802 414	47.18 %	180 492	48.64 %
between 0.02 and 0.03 [pC]	952 703	24.94 %	92 218	24.85 %
between 0.03 and 0.04 [pC]	476 033	12.46 %	45 699	12.31 %
between 0.04 and 0.05 [pC]	244 188	6.39 %	22 040	5.94 %
between 0.05 and 6 [pC]	251 670	6.59 %	21 339	5.75 %
	Value	Units	Value	Units
Average value of the charges exchanges	0.0249	pC	0.0242	pC
Average area of contact	3.7568	nm^2	3.5906	nm^2
Average time of contact	29.747	μs	31.119	μs
Minimum value of the charges exchanges	0.0079	pC	0.008	pC
Minimum area of contact	0.994	nm^2	0.829	nm^2
Minimum time of contact	6.83	μs	7.08	μs
Maximum value of the charges exchanges	5.26	pC	1.2	pC
Maximum area of contact	4.75	nm^2	4.62	nm^2
Maximum time of contact	14.6	ms	3.3	ms

Table 2.15: Collected data of charge exchange during wall collisions for different mass flow rates.

Finally, bases on the simulations results, we can conclude that the mass flow rate of powder does not impact a lot the electrification. The accumulated charged of the powder is directly proportional to the number of particles injected. Nevertheless, with a higher mass flow rate, fewer particles will undergo collisions with the wall but the percentage of particles that experience two or more collisions is higher.

2.4 Effect of different material properties

In this section, the simulations results about the electrification of powder made of different materials will be analysed. The variations will occur via the mechanical properties of the materials. The diameter and the mass flow rate have been fixed to 300 μm and 10 g/s respectively. To compare with the nominal case made of PMMA, two polymers material were chosen : Polypropylene (PP) and Polycarbonate (PC). Table 2.16 below summarises the different properties of each material :

Properties	PMMA	PP	PC
Poison ratio [-]	0.4	0.41	0.39
Young Modulus [MPa]	3000	1300	2400
Density [kg/m^3]	1090	900	1200

Table 2.16: Materials properties for the PMMA, PP and PC

The parameter that is the most difficult to estimate is the powder resistivity. It could range over many orders of magnitude depending on the ambient conditions and the particles surface. Based on the arguments of John et al.[15], in the simulations presented in this section, the resistivity has been reduced at 8.10^8 Ωm. This value is still characteristic for an insulator and the condition for an insulator that $\Delta t \ll \tau$ is well respected with this assumption.

As in the previous case, because the mass flow rate has been kept constant and due to the difference of density, the number of injected particles will be different for each simulation:

$$\dot{m} = \frac{N\ V_p\ \rho}{\tau} \quad \Leftrightarrow \quad N\rho = constant, \tag{2.3}$$

When the density is lighter than the nominal case, the concentration at the inlet will be higher. The number of particles at the inlet for the PP and the PC are respectively **828 502** particles and **621 175** particles.

2.4.1 Electrical charges on the powder at the outlet and numbers of collisions with the wall

Table 2.18 summarises the results for the charges carried by the particles at the outlet and for the number of collisions occurring with the pipe. These results for the charges carried are illustrated in Figure 2.24 below.

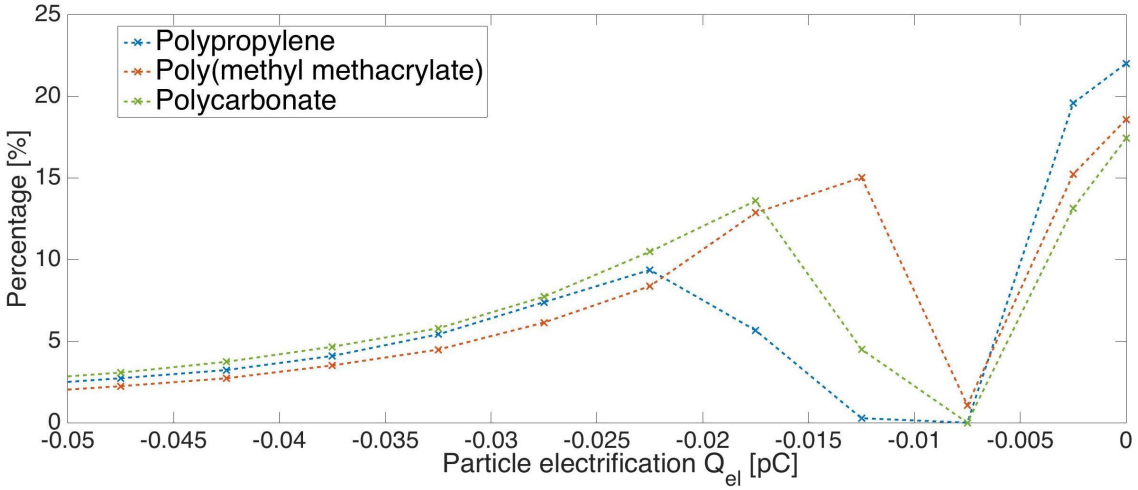

Figure 2.24: Distribution of particle electrification for different materials powder. The x-axis corresponds to the electric charge. The y-axis corresponds to the percentage of particles carrying a given charge.

If we look back at the equations of charge exchange with the wall, we can see that the parameter α_2 (Eq.1.28) will be the most affected by the change of mechanical properties. The variations depend on the density and the elastic behaviour of the material. Table 2.17 summarises the values of the elasticity parameter on the first line and the second line takes account the density. Because the Young modulus of polymer is lower than the one of steel, the elasticity parameter of the powder will be more important in the α_2 variations. For this reason, the elasticity parameter of the steel pipe is not taken into account in this table.

	PMMA	PP	PC
$(1-\nu_p^2)/E_p$	2.8 10^{-10}	6.4 10^{-10}	3.5 10^{-10}
$\rho(1-\nu_p^2)/E_p$	3.09 10^{-7}	5.76 10^{-7}	4.2 10^{-7}

Table 2.17: Elasticity parameters for the PMMA, PP and PC

	PP Powder		PC Powder	
	Number of particles	Percentage	Number of particles	Percentage
Total number of particles found at the outlet	621 941	100 %	458 310	100 %
Particles carrying charges	485 111	78 %	378 501	82.59 %
Particles carrying no-charges	136 830	22 %	79 809	17.41 %
Charge range				
between -50 and -0.1 [pC]	44 015	7.08 %	13 535	2.95 %
between -0.1 and -0.05 [pC]	82 380	13.25 %	59 556	12.99 %
between -0.05 and -0.025 [pC]	143 076	23 %	115 138	25.12 %
between -0.025 and -0.01 [pC]	93 944	15.01 %	130 103	28.38 %
between -0.01 and 0 [pC] (value 0 exclude)	121 696	19.56 %	60 169	13.13 %
Number of wall collision				
0 collision	258 526	41.57 %	139 978	30.54 %
1 collision	297 533	47.84 %	264 883	57.8 %
2 collisions	52 023	8.36 %	47 114	10.28 %
3 collisions	9 813	1.56 %	5 422	1.18 %
more than 4 collisions	4 046	0.65 %	913	0.2 %
Maximum number of collisions	56	-	21	-
	Value	Units	Value	Units
Average value of the charges carried by the particles	-0.0317	pC	-0.027	pC
Absolute value of the maximum charge carried	27.3	pC	3.44	pC
Particles undergoing no collision	Value	Units	Value	Units
Percentage of particles carrying charges	19.57 %	-	13.13 %	-
Average value of the charges carried	-8.75e-7	pC	-3.406e-7	pC
Absolute value of the maximum charge carried	1.4e-3	pC	3.59e-4	pC

Table 2.18: Collected data for the carried charges and the number of collisions at the pipe outlet for the different materials of powder.

Because the polypropylene has a Young Modulus more than two times smaller than that of PMMA, the deformation will be higher for the same compression against the wall. This appears clearly in the table and even if the density is smaller, at the end, the PP will have the higher α_2 parameter as function of the particle velocity. This means that the contact area can be higher due to the larger deformation, which leads to higher charge exchange during collisions. It appears directly in Figure 2.24 with larger percentage of particles carrying higher magnitude of charge in the distribution of the PP powder.

On the other hand, the percentage of particles carrying no or very small charge is higher for the PP powder. This is due to the density difference which induces different gravitational acceleration. Heavier particles collide more often with the bottom wall. It can be seen in the third section of the table that more particles will undergo collisions for the PC powder. The majority only collide one or twice with the wall. The PP powder shows a higher maximum number of wall-collisions and the percentage of particles undergoing more than two collisions is slightly larger. The combination of these two phenomena leads to an increased of the magnitude of the average charge carried.

Nevertheless, the change in density has less impact than the difference of elasticity parameter as it can be seen in Figure 2.25. These graphs show the charge exchange increase and accumulated charge exchange as a function of the number of collision. The three simulations reach the plateau shape around the same number of collisions. The polypropylene reaches a higher value of accumulated charge, two times higher than the PMMA.

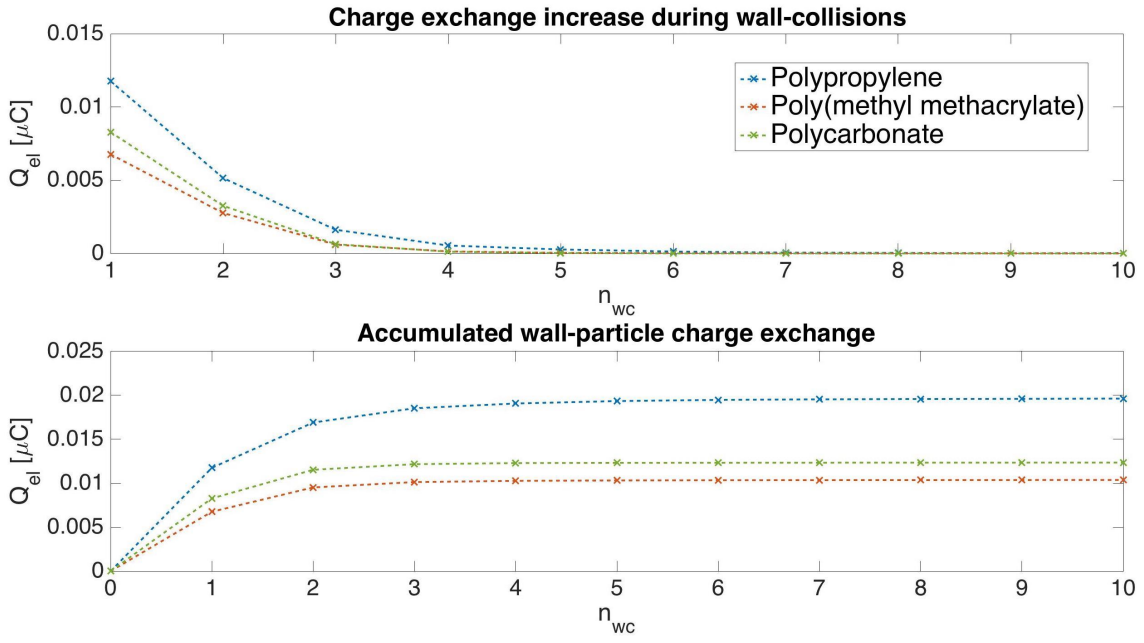

Figure 2.25: Charge exchange increase and accumulated charge exchange during wall-collisions for different materials powder : the accumulated charge at n_{wc} = i is the addition of the accumulated charge at n_{wc} = i-1 and the charge exchange increase at n_{wc} = i.

The charges are distributed on the surface of the powder and because the number of injected are different in each simulations, Figure 2.26 shows the gained and accumulated charge normalise by the whole powder surface. The trend stays the same with the PP powder accumulating more

charge but the gap between each materials is reduced.

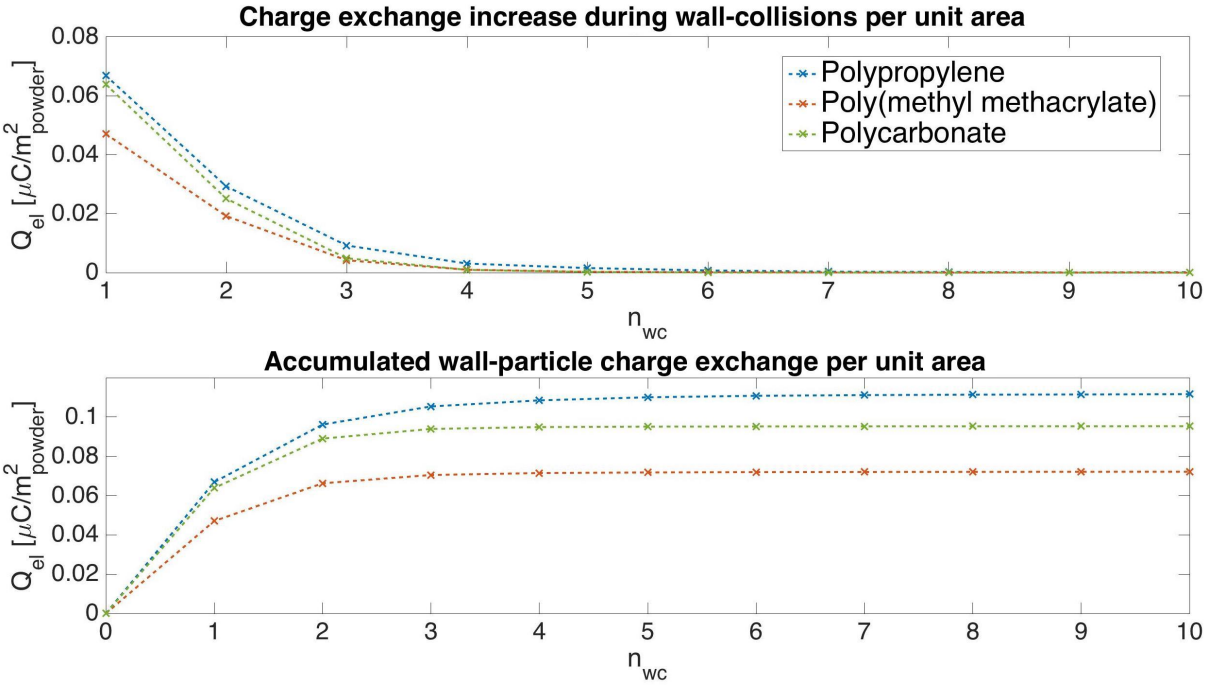

Figure 2.26: Normalisation of the charge exchange increase and accumulated charge exchange during wall-collisions for different materials powder : the accumulated charge at n_{wc} = i is the addition of the accumulated charge at n_{wc} = i-1 and the charge exchange increase at n_{wc} = i.

2.4.2 Magnitude of the charge exchange during wall collisions

The results for the charge exchange during wall collisions are summarised in Table 2.19. The range of charge exchange has been subdivided in the first section of Table 2.19 and Figure 2.27 shows the distributions of charge exchange for the different materials of the powder.

The second section of the table gives the average, minimum and maximum charge exchange. It can be seen that the average exchange charge is higher for the polypropylene powder than the two others. Nevertheless, the maximal value does not vary a lot and the charge exchange stays in the same order of magnitude.

The majority of collisions for the PP powder leads to an higher magnitude of the charge exchange but the values are more distributed over the whole range compare to the two others materials. Because the PP particles can undergo a larger deformation, the contact surface will be slightly increased.

	PP Powder		PC Powder	
	Number of collisions	Percentage	Number of collisions	Percentage
Total number of collisions with the wall	851 934	100 %	696 115	100 %
Charge exchange range				
between 0 and 0.02 [pC]	100 046	11.74 %	229 077	32.9 %
between 0.02 and 0.03 [pC]	260 500	30.58 %	206 650	29.69 %
between 0.03 and 0.04 [pC]	164 594	19.32 %	110 801	15.92 %
between 0.04 and 0.05 [pC]	109 762	12.88 %	64 938	9.33 %
between 0.05 and 0.1 [pC]	187 810	22.05 %	78 497	11.28 %
between 0.1 and 5 [pC]	29 222	3.43 %	6 152	0.88 %
	Value	Units	Value	Units
Average value of the charges exchanges	0.0416	pC	0.0308	pC
Average area of contact	4.3435	nm^2	4.2233	nm^2
Average time of contact	45.951	μs	32.788	μs
Minimum value of the charges exchanges	0.0129	pC	0.0102	pC
Minimum area of contact	1.08	nm^2	1	nm^2
Minimum time of contact	8.81	μs	7.82	μs
Maximum value of the charges exchanges	3.17	pC	3.62	pC
Maximum area of contact	5.9	nm^2	5.33	nm^2
Maximum time of contact	6.3	ms	5.7	ms

Table 2.19: Collected data for charge exchange during wall collisions for the different materials of powder.

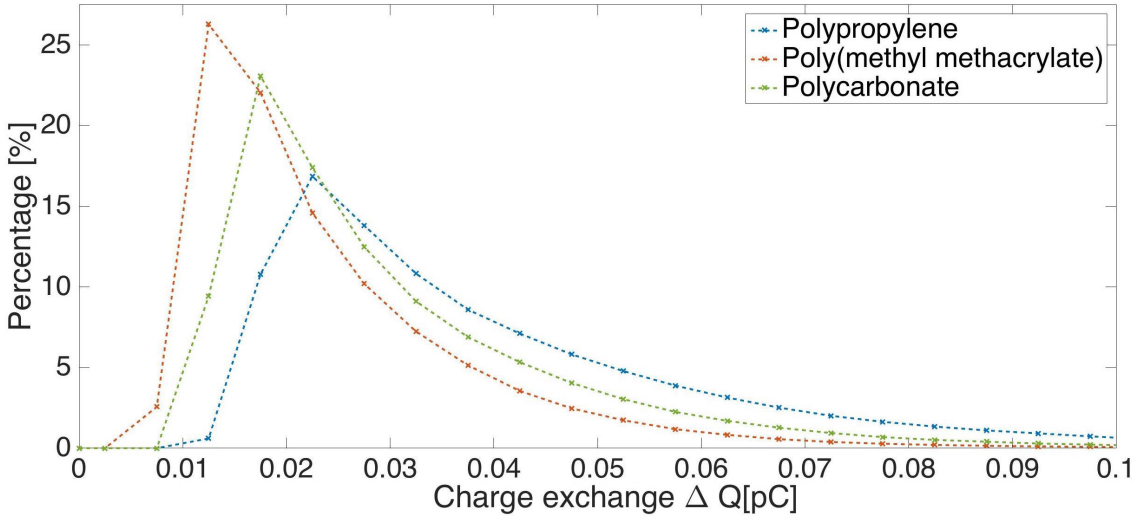

Figure 2.27: Distribution of charge exchange during wall-collisions for different materials powder. The x-axis corresponds to the electric charge. The y-axis corresponds to the percentage of collisions exchanging a given charge.

2.5 Effect of the inlet velocity

In this section, we are interested in looking how the powder electrification is affected by the fluid flow-rate, hence the turbulence intensity. To achieve this, the simulations take account of different Reynolds numbers. In the nominal case, the fluid velocity is fixed to 30 m/s given a Reynolds number around 82 192. Three others bulk velocity values were choose : 10, 20 and 40 m/s. These correspond to the following Reynolds number : give for the Reynolds number the following values : 27 397, 54 794 and 109 589.

For these simulations, it seems more intuitive to have the same number of injected particles number. To ensure the convergence, the CFL number is fixed but it depends on the fluid velocity:

$$C = \frac{u\Delta t}{\Delta x}. \tag{2.4}$$

Because of that, the time step of the simulation changes and this situation yields at different number of injected particles. Let's introduced a new variable, J_N, as the flux of injected particles:

$$J_N = \frac{N}{n_{it}\Delta t}. \tag{2.5}$$

N is the final number of particles at the inlet, n_{it} the number of iteration and Δt the time step. The mass flow rate can also be expressed depending on this parameter as

$$\dot{m} = J_N \; V_p \; \rho_p \tag{2.6}$$

To keep the same number of particles when the fluid velocity decreases, the particles flux and the mass flow rate will also decrease. Table 2.20 shows for each simulations the values of the flux

and the mass flow rate.

Velocity [m/s]	10	20	30	40
J_N [particles/s]	233 000	467 000	700 000	933 000
$\dot{m}$ [g/s]	3.33	6.7	10	13
Δt	5.866E-5	2.935E-5	1.954E-5	1.466E-5
Number of particles at the inlet	683 192	685 192	684 168	683 946

Table 2.20: Input data for the fluid velocity variations

2.5.1 Electrical charge of the powder at the outlet and number of collisions with the wall

The results for the electrical charge on the powder at the outlet and the number of collisions occurring with the wall can be found in Table 2.21. In the first section of this table, it can be noticed that more particles leave the pipe for case of the higher velocity value but also the percentage of electrically charged particles is higher.

The second section gives information about the range of carried charge. The values are in the same order of magnitude for all the simulations but some variations occur in the percentage of each subdivision. These results are illustrated in Figure 2.28. The point on the graph between -0.005 pC and 0 represents the percentage of particles charge via inter-particle collisions mechanism. It is smaller for the case of the lowest Reynolds number and do not vary a lot for the three others cases.

The peak of each distribution increases in charge magnitude when the fluid velocity increases. This comes directly from the equation of α_2 (Eq.1.28) : when the particles velocities increase, the contact area becomes larger and results in higher charge exchange. The percentage of particles carrying small charge is then reduced when the fluid velocity increases.

The third part of the table gives the percentages of particles undergoing different number of collisions with the wall. Except for the case of the inlet velocity at 10 m/s, around 33 % of the powder do not interact with the wall and more than half of the powder only collide one time. For the case of the lowest Reynolds number, more than 25% of the particles undergo several collisions and we can see that the maximum number of collisions increases when the velocity decreases. The gain of charge during collision with the wall is slightly lower for the lowest Reynolds number case, but because of these multiple impact, some particles will be more heavily charged. This can be seen in the next section of the table about the maximum charge carried. This can explain why the average charge carried have very close values even if the exchange is lower when the velocity decreases.

	u_{air} = 10 m/s		u_{air} = 20 m/s		u_{air} = 40 m/s	
	Number of particles	Percentage	Number of particles	Percentage	Number of particles	Percentage
Total number of particles found at the outlet	403 730	100 %	495 907	100 %	511 195	100 %
Particles carrying charges	278 604	69.01 %	387 735	78.19 %	419 458	82.05 %
Particles carrying no-charges	125 126	30.99 %	108 172	21.81 %	91 737	17.95 %
Charge range						
between -7 and -0.05 [pC]	46 365	11.48 %	30 839	6.22 %	70 512	13.79 %
between -0.05 and -0.025 [pC]	51 459	12.75 %	71 033	14.32 %	112 395	21.99 %
between -0.025 and -0.005 [pC]	141 390	35.02 %	212 357	42.82 %	158 291	30.96 %
between -0.005 and 0 [pC] (value of 0 exclude)	39 390	9.76 %	73 506	14.83 %	78 260	15.31 %
Number of wall collision						
0 collision	159 844	39.59 %	181 678	36.63 %	169 997	33.25 %
1 collision	115 250	28.55 %	252 497	50.92 %	284 835	55.72 %
2 collisions	31 166	7.72 %	44 831	9.05 %	49 944	9.77 %
3 collisions	23 540	5.83 %	10 482	2.11 %	5 779	1.13 %
more than 4 collisions	73 930	18.31 %	6 419	1.29 %	640	0.13 %
	Value	Units	Value	Units	Value	Units
Average value of the charges carried by the particles	-0.0188	pC	-0.0161	pC	-0.0244	pC
Absolute value of the maximum charge carried	5.63	pC	6.32	pC	1.93	pC
Maximum number of collisions	66	-	59	-	17	-
Particles undergoing no collision						
Percentage of particles carrying charges	8.6 %	-	14.82 %	-	15.3 %	-
Average value of the charges carried	-1.7306e-7	pC	-1.4279e-7	pC	-3.3708e-7	pC
Absolute value of the maximum charge carried	4.08e-4	pC	1.61e-4	pC	5.82e-4	pC

Table 2.21: Collected data for carried charges and the number of collisions at the pipe outlet for the fluid velocity variations.

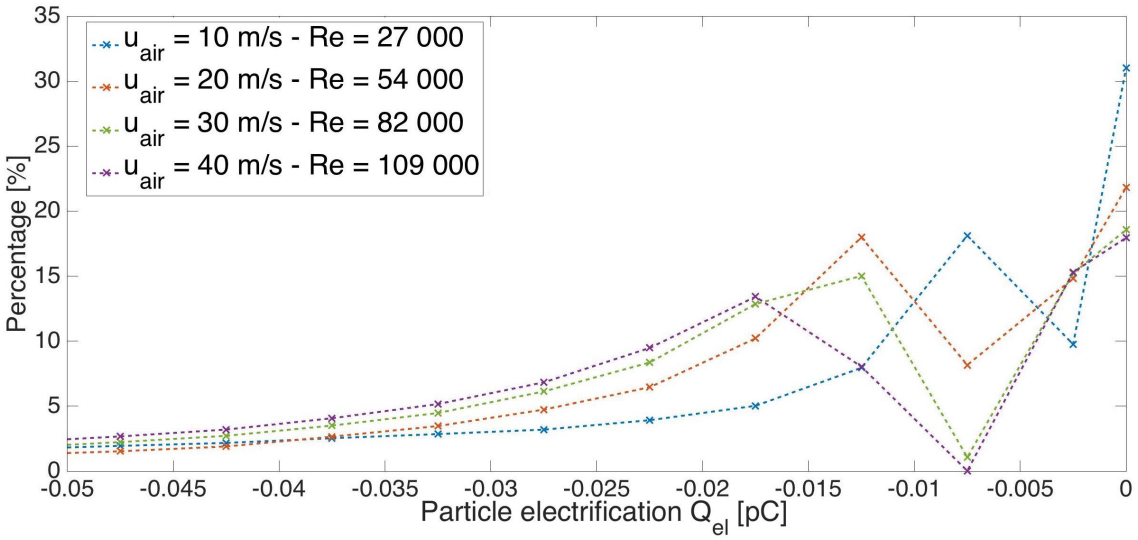

Figure 2.28: Distribution of particle electrification for different inlet velocities. The x-axis corresponds to the electric charge. The y-axis corresponds to the percentage of particles carrying a given charge.

Figure 2.29 shows a comparison of the charge exchange increase and accumulated charge exchange during wall-collisions. Because a large number of particles go through more than three impacts with the wall, the case with the lowest Reynolds number has a small increase of charge per number of collision until $n_{wc} = 15$. Because of this constant gain, the plateau shape curve will only appear after ten collisions.

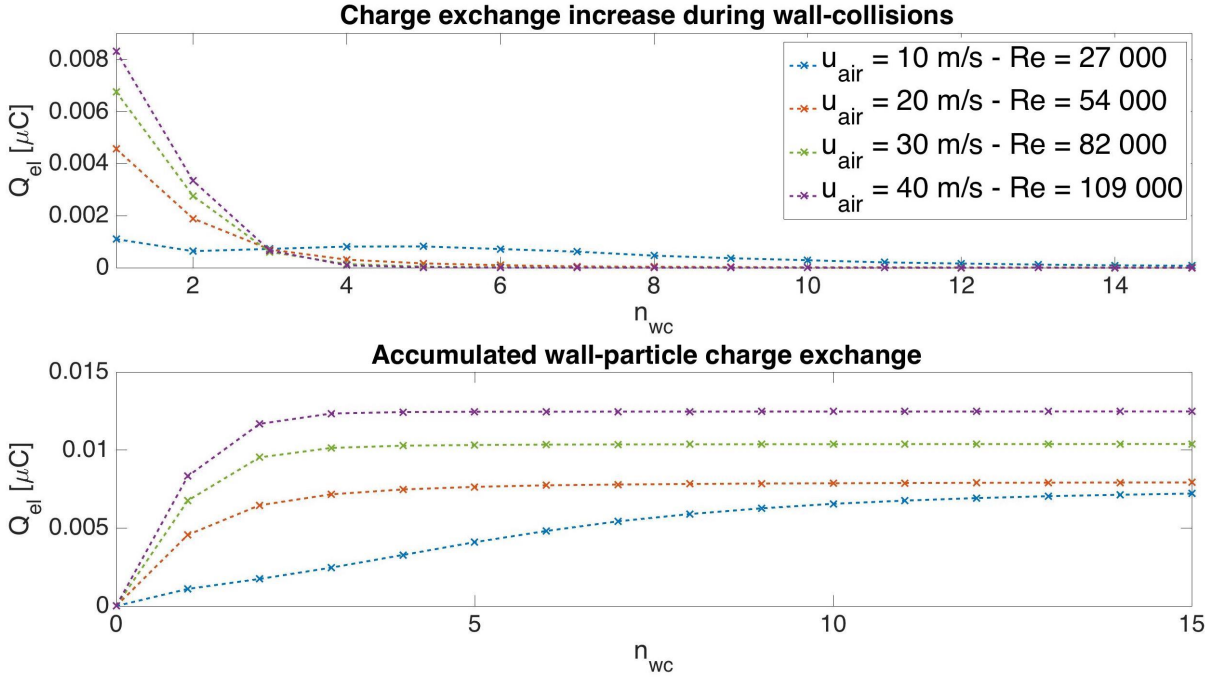

Figure 2.29: Charge exchange increase and accumulated charge exchange during wall-collisions for different inlet velocities : the accumulated charge at n_{wc} = i is the addition of the accumulated charge at n_{wc} = i-1 and the charge exchange increase at n_{wc} = i.

At the end, it shows that the accumulated charge is more important when the fluid velocity is larger but the accumulated value of the case of the inlet velocity at 10 m/s velocity tends to

reach nearly the value for the case of 20 m/s inlet velocity.

With faster fluid flow, more particles leave the pipe leading to a larger powder surface at the outlet. Figure 2.30 shows the charge exchange increase and accumulated charge exchange during wall-collisions normalised with the powder surface. In the case of the smallest inlet velocity, the accumulated charge attains a higher value and exceeds the value of the case of 20 m/s inlet velocity. The fact more that there is a higher number of particles subject to multiple collisions is due to the low fluid velocity. The particle velocities are also reduced in this case.

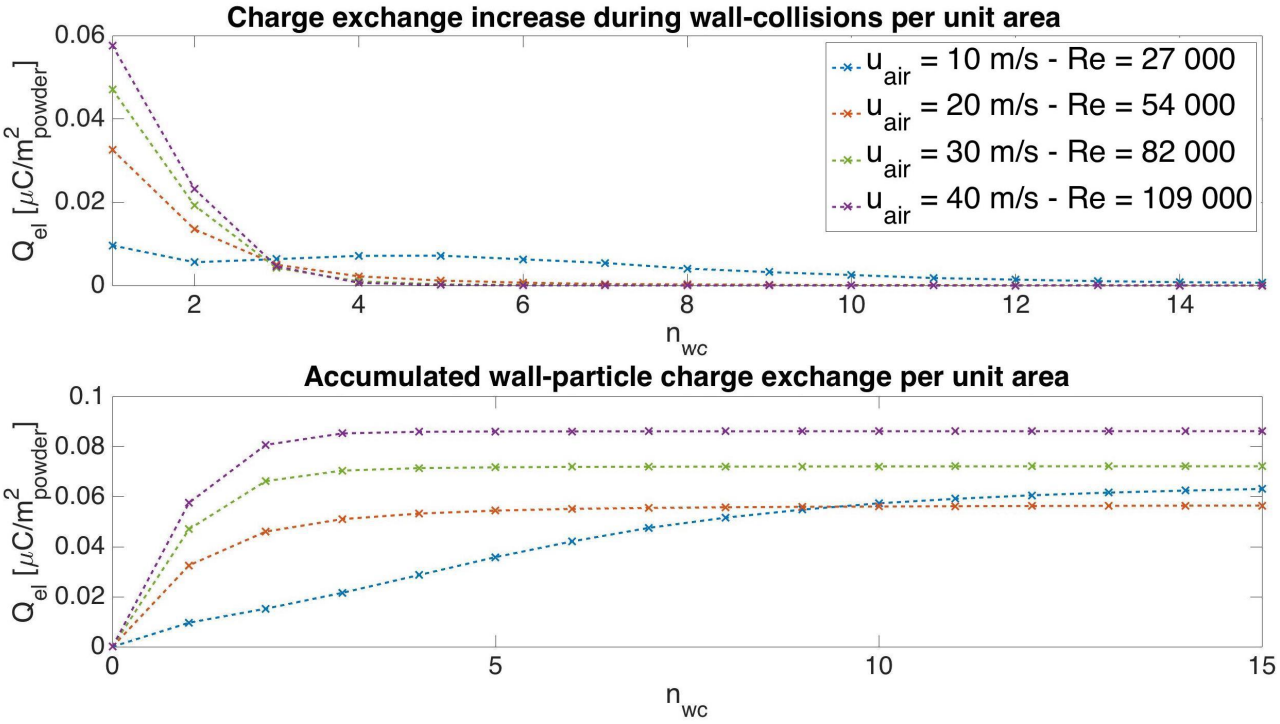

Figure 2.30: Normalisation of the charge exchange increase and accumulated charge exchange during wall-collisions for different inlet velocities : the accumulated charge at n_{wc} = i is the addition of the accumulated charge at n_{wc} = i-1 and the charge exchange increase at n_{wc} = i.

As it can be seen in Figure 2.31, at the end of the pipe, the particles are settle down. The gravity and drag forces reduce the acceleration of the powder and make it collide more often with the pipe. Because of that, the total number of collision is double time higher in this case as it can be seen in Table 2.22.

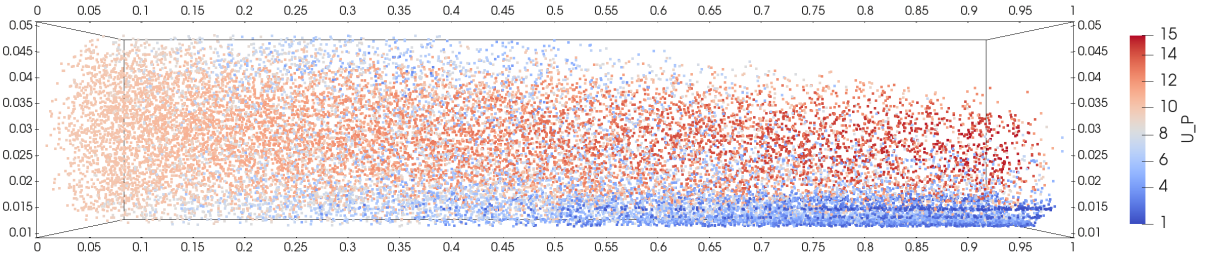

Figure 2.31: Visualisation of the particles velocities for the fluid velocity equal to 10 m/s at t = 1s. For better visualisation, the radial coordinate is scaled by a factor five.

To take into account this difference of behaviour, an other normalisation of the graph has been made with the use of the total number of collisions. The numbers of particles at the outlet do not change more than 20 % between the case of the low and high inlet velocities. Figure 2.32 shows the gained and accumulated charge per impact.

This time, the case of lowest fluid velocity reaches also smallest values of accumulated charge. As mentioned before, the charge exchange increased with the velocity and this is well represented in this last graph. Nevertheless, we can see that the variation per impact is small, less than 0.1 pC. Because the velocity is lower, particles will stay longer in the pipe and can undergo more collision. Below a certain value, the gravity acceleration becomes important and the particles form a layer in the bottom of the pipe.

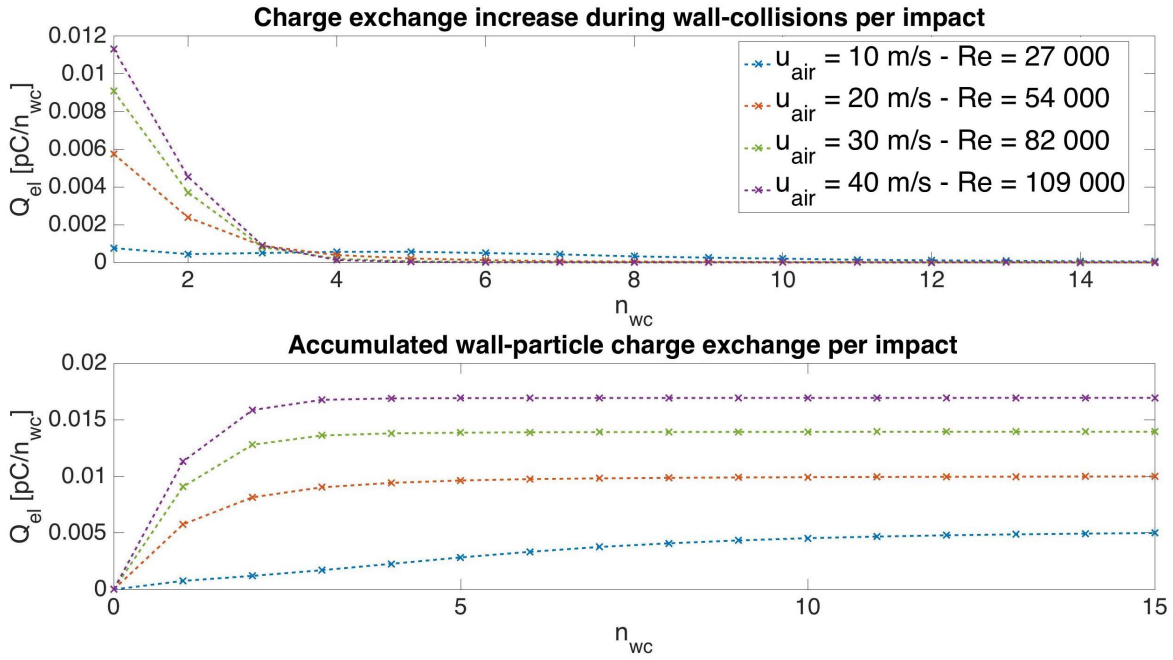

Figure 2.32: Normalisation of the charge exchange increase and accumulated charge exchange during wall-collisions for different inlet velocities : the accumulated charge at n_{wc} = i is the addition of the accumulated charge at n_{wc} = i-1 and the charge exchange increase at n_{wc} = i.

On the basis of these two observations, it can be claimed that by decreasing the fluid velocity, the particles undergo more collisions with the pipe. Because of that, the powder could be more heavily charged even if the increase of velocity will increase the amount of charge transferred during electrification contact as it would be seen in the next section.

2.5.2 Magnitude of the charge exchange during wall collisions

In this section, we will analyse the results for the charge exchange during wall collision. The results are summarised in Table 2.22. As mentioned before, the number of collisions increases

	u_{air} = 10 m/s		u_{air} = 20 m/s		u_{air} = 40 m/s	
	Number of collisions	Percentage	Number of collisions	Percentage	Number of collisions	Percentage
Total number of collisions with the wall	1 444 663	100 %	792 863	100 %	736 108	100 %
Charge exchange range						
between -0.01 and 0 [pC]	6	< 0.01 %	-	-	-	- %
between 0 and 0.01 [pC]	884 212	61.2 %	115 567	14.57 %	577	0.08 %
between 0.01 and 0.02 [pC]	515 978	35.72 %	416 852	52.58 %	286 773	38.96 %
between 0.02 and 0.03 [pC]	31 375	2.17 %	169 967	21.44 %	202 800	27.55 %
between 0.03 and 0.04 [pC]	7 431	0.51 %	60 328	7.61 %	105 232	14.29 %
between 0.04 and 0.05 [pC]	2 754	0.19 %	17 935	2.26 %	60 404	8.21 %
between 0.05 and 6 [pC]	2 907	0.2 %	12 214	1.54 %	80 332	10.91 %
	Value	Units	Value	Units	Value	Units
Average value of the charges exchanges	0.0098	pC	0.0186	pC	0.029	pC
Average area of contact	1.187	nm^2	2.5052	nm^2	4.5951	nm^2
Average time of contact	37.709	μs	34.368	μs	28.888	μs
Minimum value of the charges exchanges	-0.0071	pC	0.0014	pC	0.0072	pC
Minimum area of contact	0.35	nm^2	0.608	nm^2	1.11	nm^2
Minimum time of contact	8.57	μs	7.46	μs	6.49	μs
Maximum value of the charges exchanges	2.51	pC	5.11	pC	1.37	pC
Maximum area of contact	1.97	nm^2	3.37	nm^2	5.86	nm^2
Maximum time of contact	19.3	ms	19.1	ms	2.8	ms

Table 2.22: Collected data of charge exchange during wall collisions for different inlet velocity

when the velocity decreases. This drop in the number of collisions is low between the three highest Reynolds number but becomes very large for the lowest one with two times more collisions. As some particles undergo several impacts, they can transport high electrical charge, and this leads to negative exchange with the wall, meaning the particles material have given electrons to the pipe material.

The third section of the table gives information about the average, minimum and maximum values of charge exchange, contact areas and contact times. It can be seen that when the fluid velocity increases, the average charge increases also. This comes directly from the increased of the parameter α_2 that represents the percentage based on the radius of contact length during maximal compression, with the velocity in the equations of exchange with the wall. Because of that, the contact area becomes more important and improves the magnitude of charge exchange. The contact time will also be impacted but this will have small contribution due to the exponential.

About the breadth, the values for these variations stay in the same order of magnitude but with difference in percentages in the subdivision of the range. These differences can be observed in Figure 2.33. The peak of the distribution reach higher values of charge exchange with the increase of velocity but the percentage is smaller. In this case, the magnitudes of the charge exchange are more distributed over the whole range.

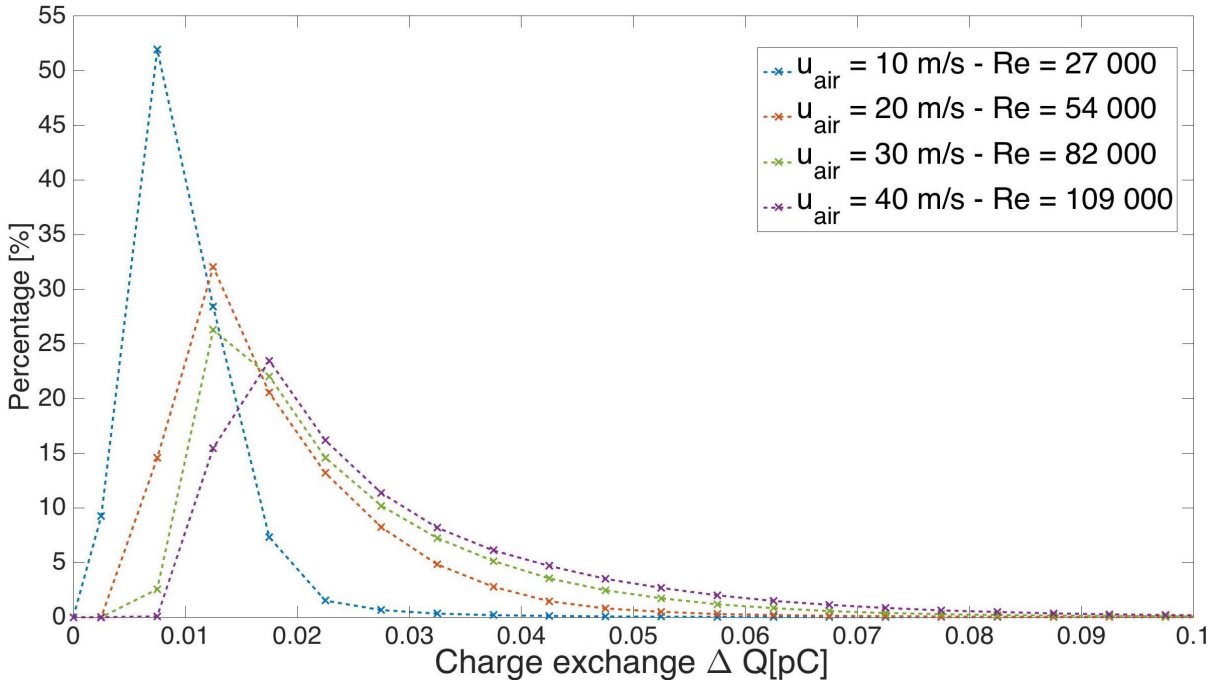

Figure 2.33: Distribution of charge exchange during wall-collisions for different inlet velocities. The x-axis corresponds to the electric charge. The y-axis corresponds to the percentage of collisions exchanging a given charge.

Chapter 3

Comparison between simulations and experiments

The purpose of this chapter is to test the validity of the simulations and compare their results with those of experimental work found in several scientific publications. Because the triboelectric charging of powders depends on many parameters, like the relative humidity, the pipe or particles materials or diameters, etc, finding experimental works based on the same geometry and materials for both pipe and particles could not be achieved. Although, a high number of books and reviews treating the subject of powder electrification in a pneumatic transport are available , especially due to the strong interest to improve the safety and efficiency of pneumatic transport systems in process engineering.

More particularly, the paper written by Khashayar Saleh et al.[16] lists the major works and presents the results of different experimental studies related to significant parameters as the particles size, the particles mass flow rate and the fluid velocity.

3.1 Comparison for the effect of particles diameter

When the diameter increases, the magnitude of the charge-to-mass ratio increases. This results directly from the exchange surface that becomes larger during the impact when the particle is larger.

In order to compare the numerical results for the diameter variations, the experimental results of Watano et al.[11][17] can be used. In these papers, the electrification of PMMA powder in a steel pipe has been measured. Some additional parameters are considered, for instance the length of the pipe or the temperature , but the experimental equipment is the closest to the parameters of the simulations performed. The comparison is illustrated in Figure 3.2 and the numerical values are given in Table 3.1. For each point, the fluid velocity is set at 30 m/s. We are interested by

looking at the trends and these values are given only for information.

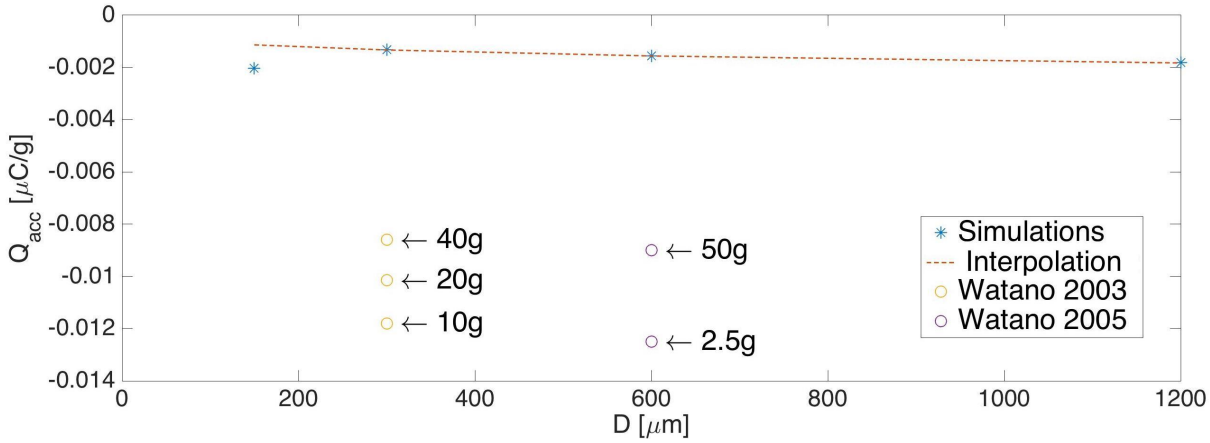

Figure 3.1: Charge-to-mass ratio as a function of particles diameter : comparison between the simulations results and experimental measurements

Simulations values			Watano et al.[11][17]		
Diameter [μm]	m [g]	Q [μm/g]	Diameter	m [g]	Q [μm/g]
150	10	0.002	300	10	0.0118
300	10	0.0013	300	20	0.01015
600	10	0.0016	300	40	0.0086
1200	10	0.0018	600	2.5	0.0125
			600	50	0.009

Table 3.1: Charge-to-mass ratio for different diameter values : comparison between the simulation results and experimental measurements

We made strong assumptions about the powder : for instance, all the particles have the same dimension and are perfectly spherical. Some articles propose a relationship between the charge and the diameter as a power-law. In the graph, the charge was interpolated by $|Q| = aR^n$ and the values of the parameters a and n are respectively -0.01 and 0.229. The results is represented by the red dotted line.

Regarding the trends, we see that the charge becomes more important when the diameter increases in the simulations. The experience of Watano (2003)[11] depicts a decrease of the charge when the mass loading become larger. We can suppose that if a quantity of 50 g of powder would have been used in the experience, the charge would have been smaller. Then for a smaller diameter, the charge should also be smaller compared to the experiment of Watano (2005)[17].

In the article by Saleh et al.[16], another type of result is presented, depending on the particles diameters. The authors take into account the first impact on the wall, since it corresponds to the maximum charge exchange when the powder has no initial charge. Then they look at the relationship between the charge and the the diameter of the particles. For their experiments, the powder is made of glass particles and two types of pipe were used : teflon (PTFE) and nylon. The experiment concludes on a relationship between the charge and the particles diameter following a power-law with an exponent equal to 1.5.

To seek if such a behaviour also appears in the simulation, the charge values corresponding to the first impact against the wall were taken for all particles diameters considered so far. Figure 3.2 illustrates the results and the red line represents the interpolation via a power law as mentioned previously ($|Q| = aR^n$). In this case, the exponent is equal to 1.7 and the parameter a = -0.07. We can see a comportment similar to the experiments of Saleh et a, while the differences can be explained by the use of different materials.

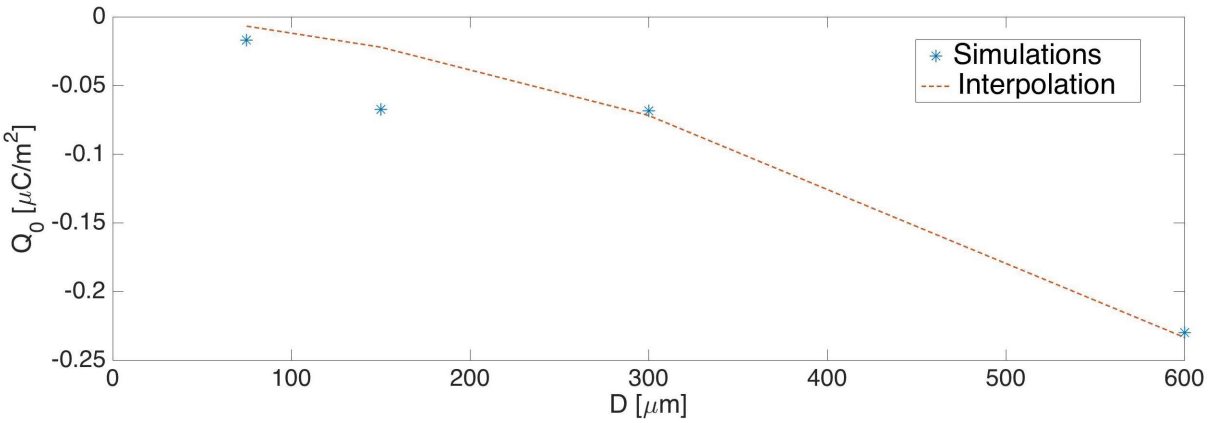

Figure 3.2: Initial charge-to-surface ratio depending on the diameter : approximation of the simulations values with a power law $Q_0 = aR^n$ with a = -0.07 and n = 1.7.

3.2 Comparison for the effect of the mass flow rate

When we increase the mass flow rate of injected particles, more impacts can occur with the wall but also more collisions between the particles. When we reach higher mass flow rates, the assumption of dilute regime is not valid anymore. In this case, we cannot suppose anymore that the particles are isolated from each other. For the particles near the wall, the probability to stay close to it is higher because the probability to collide another particle and be redirected to the wall is higher. Additionally more particles will impact several times the wall and because of the charge on the particle itself, the charge exchange with the wall will decrease at each impact. This can be an explanation for the decrease of the powder charge when the mass flow rate increases.

Three articles have been found about the electrification of a powder with mass flow rate variations. The first two are from Watano et al.[11] and from Schwindt et al.[18]. The experiments used a PMMA powder with a mean distribution size near 300 μm and the fluid velocity was set at 30 m/s. The results of the experiments can be found in Table 3.2. We see that the powder charge decreases when the mass flow rate increases. In the simulations, we have a decrease around 0.7 pC/g per g, while Watano is around 107 pC/g per g and, Schwindt is around 2.55 pC/g per g.

Saleh et al.[16] also made experiments with mass flow rate variations. They conclude that the mass flow rate does not affect the electrification: they explain that the linear increase of charge exchange comes from the fact that more particles are available that can impact the wall. When normalised to the surface area of the powder, the experimental results show a relatively constant

Simulation values		Watano et al.[11]		Schwindt et al.[18]	
m [g]	Q [μm/g]	m [g]	Q [μm/g]	m [g]	Q [μm/g]
5	0.0013498	10	0.0118	186	0.0031
10	0.0013239	20	0.01015	382	0.0026
50	0.0013174	40	0.0086		

Table 3.2: Charge-to-mass ratio for different powder mass values : comparison between the simulation results and experimental measurements

value for the charge to surface ratio.

3.3 Comparison for the effect of the inlet fluid velocity

All publications cited agree that the flow regime, laminar or turbulent, has a strong influence on the electrification of a powder. Watano et al.(2003)[11] and Grosshans and Papalexandris[2] show that the charge-to-mass ratio increases with the fluid velocity until a certain value at which the charge then starts to decrease with the fluid velocity. When the velocity becomes higher, the number of impacts against the wall decreases and leads to a lower charge exchange.

Figure 3.3 shows the comparison between the experimental results of Watano et al. (2003) and previous simulations made by Grosshans and Papalexandris (2016). The same program was used for these simulations and the only difference comes from the resistivity of the PMMA powder taken as 10^{16} Ωm in the case of Grosshans and Papalexandris (2016). The total mass of the powder in each case is 10 g.

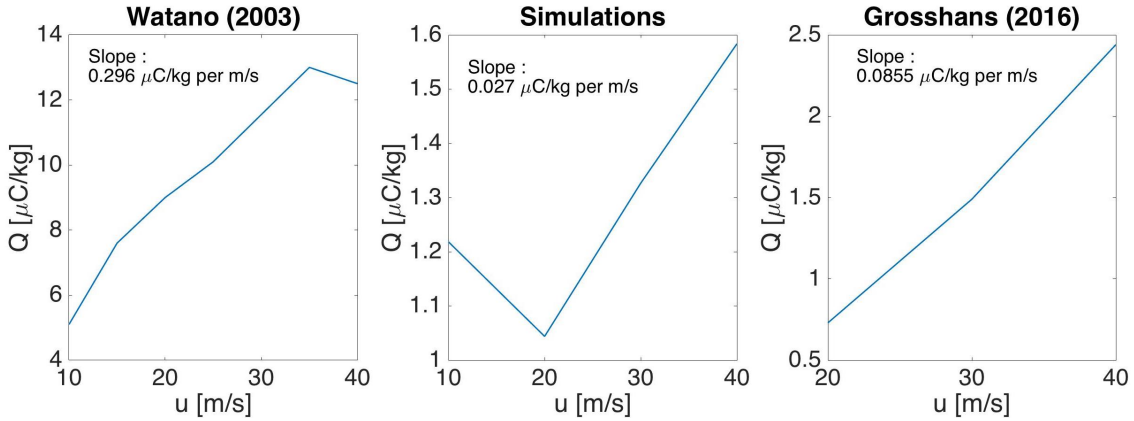

Figure 3.3: Charge-to-mass ratio as a function of the fluid velocity. Comparison of various litterature sources.

In our simulations, the lowest velocity case shows another behaviour : at a velocity of 10 m/s, the assumption of dilute regime is not valid anymore, and the particles pile up at the end of the pipe, increasing the number of collisions, and the powder is more charged at the outlet. The experiment does not show this trend even if the pipe is twice longer. Furthermore, Saleh et al. made experiments on a larger scale of air velocity, from 5 m/s to 44 m/s. The low velocity

behaviour mentioned above appears below 7 m/s. In these experiments, the pipe is 0.5 m long with a diameter of 1 cm . Due to the simplified case and hypothesis made, the change of transport regime occurs at a lower velocity then in our simulations.

In the experiments of Watano (2003)[11], we identify a decrease of charge-to-mass ratio at high velocity . This trends is also appearing in experiments of Schwindt et al.[18]. At higher velocity, the transport of powder become more uniform and less impacts will happen with the wall. In our simulations, all the particles have the same shape and volume. In reality, because of the PSD, particle size distribution, and of the decreasing air resistance with the diameter, the particles move at different velocities, the lighter one moving faster. We have then a transportation velocity differential that will affect the way the particles impact the wall. The peak of higher charge exchange as function of the velocity is located between 30 and 40 m/s in the experiment of Watano (2003). In our simulations, we did not examine the effect of velocity between 30 and 40 m/s. A simulation with a inlet velocity in this range could have been show if the transition also appears or not.

3.4 Effect of the powder material properties

The electrical charging of the powder depends on many parameters and the way the powder material impacts it is not yet well explained. The mechanism of exchange itself has been discussed in many articles. Instead of the classical electron transfer, some articles propose the idea of ion transfer or even material transfer when the powder is contaminated by small dust or impurities on the surface [19]. Nevertheless, all articles agree to the increase of charge exchanges when the contact surface is larger.

The triboelectric charging depends on the surface properties and due to the size of the particles, impurities and defects can have an influence on the behaviour of charge exchange. Also, when the powder is prepared, various parameters can influence the surface properties.

For a polymer powder, depending on the conditions of the flow and on the pipe material, the charge exchange can be negative or positive, which results in, the presence of donor and acceptor sites on the surface. The distribution of state of polymeric materials are not easy to determine and quantum chemistry calculations are needed to reach accurate solutions.

The triboelectric series in Table 3.3 lists materials in a sequence allowing to determine the sign of the charge gain when two different material are in contact. When considering two materials from this table, the one with highest position in the table will gain positive charge while the other one, at the lowest position in the table, will gain negative charge.

This type of table is based on experiments and on chemical properties of the material, for instance the electronegativity. Nevertheless, depending of the source, the position of some polymeric materials in the list may vary [20]. This suggests that the charging of the powder is not only

Positive +
Air
Nylon
Aluminum
Steel
Wood
PMMA
Gold
Polycarbonate
Polypropylene
Negative -

Table 3.3: Triboelectric series [20] - partly given

linked to the intrinsic properties of the material but that other physical parameters can influence this charging, for instance the defect in the surface .

Conclusions

The aim of this master's thesis was to understand the electrification of a powder in a pneumatic transport based on results from numerical simulations and on the comparison with experiments. Four parameters have been selected for this purpose : the particles diameter, the particles mass flow rate, the particles material and the fluid velocity.

The diameter variation results in a decrease of the mass-to-surface ratio during the transport, if a constant weight of powder is injected. The charge exchange shows a large decrease, about one order of magnitude when the diameter is divided by two. Because the volume is kept constant, the surface available for the smallest particles is larger. Due to that and to the fact that particles are lighter when smaller, they experience more impacts with the wall. The smallest diameter tends to have higher electrification at the outlet although the charge exchange is smaller. The simulation results and the experiments suggest a relation between the charge and the diameter following a power law but the value of the exponent could not be determined precisely.

The mass flow rate variations were performed by changing the mass flow rate of the particles at the inlet. The results show an increase of the charge-to-mass ratio when the mass flow rate decreases. This trend also appears in the experimental studies found in different publications. The simulation shows only a slight drop while experimental measurements show a more important difference. Nevertheless, this difference stays small, less than 1 μC/g per g of powder, showing the small impact of the particle mass flow rate on the electrification.

About the results from changing the powder material, several approximations have been made. Moreover, due to the lack of experimental work on this parameter, we cannot compare the simulation to practical results. The simulation results suggest a larger charge exchange when the Young modulus of the material is smaller. Such a material can undergo larger deformation during the impact, increasing the surface of the capacitor in the model used to calculate the charge exchange. Also, if the material has a smaller density, the powder can experience more multiple impacts with the wall and at the end, be globally more charged.

Finally, the simulations of different fluid velocities are compared to the experiments. The turbulent regime has a strong link with the electrification of a powder : in that case the powder becomes more charged when the Reynolds number increases. This was evidenced in the simulation : at very high fluid velocity, the particles velocity during impact is higher and the charge exchange

is thus also higher. The experiments show, at high velocity, a decrease of charge exchange due to a decreasing number of wall-collisions. This was not appearing in our simulation results, although some numerical model results at fluid velocities between 30 and 40 m/s could give information about the appearance of a transition.

We can conclude by saying that the charging of a powder during pneumatic transport depends strongly on the particles size and of the transporting fluid conditions. Working at low velocity with particles of low diameter decreases the electrification phenomena. Nevertheless, under certain values of velocity and particles diameter, the change of transport regime shows the inverse, i.e. an increase of the charging process. The mass flow rate has a small impact and by increasing the particle mass flow rate, the charge over the powder can be reduced. This increase is limited by the constraint of keeping a dilute regime. The choice of parameters should thus be considered with great care and attention.

List of Figures

List of Tables

Bibliography

[1] Numerical study of the influence of the powder and pipe properties on electrical charging during pneumatic conveying. *Powder Technology*, 315:227–235, 2017.

[2] Holger Grosshans and Miltiadis V. Papalexandris. Evaluation of the parameters influencing electrostatic charging of powder in a pipe flow. *Journal of Loss Prevention in the Process Industries*, 43:83–91, 2016.

[3] Holger Grosshans and Miltiadis V. Papalexandris. Direct numerical simulation of triboelectric charging in particle-laden turbulent channel flows. *Journal of Fluid Mechanics*, 818:465–491, 2017.

[4] Holger Grosshans and Miltiadis V. Papalexandris. Large eddy simulation of triboelectric charging in pneumatic powder transport. *Powder Technology*, 301:1008–1015, 2016.

[5] S. Matsusaka, H. Maruyama, T. Matsuyama, and M. Ghadiri. Triboelectric charging of powders: A review. *Chemical Engineering Science*, 65(22):5781–5807, 2010.

[6] Schiller L. and Naumann A. A drag coefficient correlation. *Z. Ver. Dtsch. Ing 77*, pages 318–320, 1933.

[7] Karl-Heinrich Grote and Jörg Feldhusen. *Dubbel* -. Springer Berlin Heidelberg, Wiesbaden, 2007. ISBN 978-3-540-68191-5.

[8] S.L. Soo. Dynamics of charged suspensions. pages 71–73, 1971.

[9] D.A. Seanor. *Electrical Properties of Polymers*. Elsevier Science, 2013. ISBN 9781483220123.

[10] Julian Scott Jean Mathieu. *An introduction to turbulent flow*. Cambridge University Press, 2000.

[11] Satoru Watano, Seiji Saito, and Teruo Suzuki. Numerical simulation of electrostatic charge in powder pneumatic conveying process. *Powder Technology*, 135-136:112–117, 2003. Electrostatic Phenomena in Particulate Processes.

[12] Massimo Germano, Ugo Piomelli, Parviz Moin, and William H. Cabot. A dynamic sub-grid[U+2010]scale eddy viscosity model. *Physics of Fluids A: Fluid Dynamics*, 3(7):1760–1765, 1991.

[13] D. K. Lilly. A proposed modification of the germano subgrid[U+2010]scale closure method. *Physics of Fluids A: Fluid Dynamics*, 4(3):633–635, 1992.

[14] R.I Issa. Solution of the implicitly discretised fluid flow equations by operator-splitting. *Journal of Computational Physics*, 62(1):40–65, 1986.

[15] W. John, G. Reischl, and W. Devor. Charge transfer to metal surfaces from bouncing aerosol particles. *Journal of Aerosol Science*, 11(2):115–138, 1980.

[16] Khashayar Saleh, Adoum Traore Ndama, and Pierre Guigon. Relevant parameters involved in tribocharging of powders during dilute phase pneumatic transport. *Chemical Engineering Research and Design*, 89(12):2582–2597, 2011.

[17] Satoru Watano. Mechanism and control of electrification in pneumatic conveying of powders. *Chemical Engineering Science*, 61(7):2271–2278, 2006.

[18] N. Schwindt, U. von Pidoll, D. Markus, U. Klausmeyer, M.V. Papalexandris, and H. Grosshans. Measurement of electrostatic charging during pneumatic conveying of powders. *Journal of Loss Prevention in the Process Industries*, 49:461–471, 2017.

[19] F. Chowdhury, A. Sowinski, M. Ray, A. Passalacqua, and P. Mehrani. Charge generation and saturation on polymer particles due to single and repeated particle-metal contacts. *Journal of Electrostatics*, 91:9–15, 2018.

[20] A.F. Diaz and R.M. Felix-Navarro. A semi-quantitative tribo-electric series for polymeric materials: the influence of chemical structure and properties. *Journal of Electrostatics*, 62 (4):277–290, 2004.

Rue Archimède, 1 bte L6.11.01, 1348 Louvain-la-Neuve **www.uclouvain.be/epl**